Physical properties and reaction kinetics of CO_2 absorption into unloaded and CO_2 loaded viscous monoethanolamine (MEA) solution

Rouzbeh Ramezani[a*], Ida M. Bernhardsen[b], Renzo Di Felice[a], Hanna K. Knuutila[b]

[a]Department of Civil, Chemical and Environmental Engineering, University of Genoa, Via Opera Pia, Genova, Italy

[b]Department of Chemical Engineering, Norwegian University of Science and Technology (NTNU), NO-7491 Trondheim, Norway

Abstract

In order to comprehensively understand how solvent free concentration and high viscosity affect mass transfer and consequently absorption flux, CO_2 absorption kinetics into unloaded and CO_2 loaded viscous monoethanolamine (MEA) solution were studied in this work using the string of discs contactor. Moreover, density and viscosity of unloaded and loaded viscous MEA solutions were measured using an Anton Paar DMA 4500 density meter and an Anton Paar Lovis 2000 ME rolling-ball viscometer, respectively, and the results were correlated using Redlich-Kister and modified Vogel-Tamman-Fulcher equations as a function of temperature, concentration and CO_2 loading. Overall mass transfer coefficients of CO_2 absorption in viscous MEA solution were measured over a wide temperature range of 298.15 to 343.15 K and CO_2 loading in the range of 0 to 0.4 (mol CO_2/mol MEA). A simplified kinetic model was applied to interpret the mass transfer data and explain reaction kinetics between CO_2 and unloaded and loaded viscous MEA solution. The effect of temperature, CO_2 loading and viscosity on second order reaction rate constant and overall mass transfer coefficients was also discussed.

Keywords: CO_2 capture; Monoethanolamine; Mass transfer; Viscosity; Reaction kinetics.

* Corresponding author: E-mail: rouzbeh.ramezani@edu.unige.it (Dr. Rouzbeh Ramezani)

1. Introduction

There is a worldwide concern over the increase in the concentration of CO_2 and its high contribution to global warming. The burning of fossil fuels for electricity is considered as one of the major sources of greenhouse gas emissions [1]. Apart from its environmental impact, CO_2 may cause problems like corrosion of steel equipment in oil and gas industry [2]. Therefore, the capturing CO_2 from gas streams from power plants not only is important from an industrial point of view, but it can also limit the emissions of greenhouse gases to the atmosphere and reduce the environmental issues.

Post-combustion capture using aqueous alkanolamine solutions is one of the most effective technologies to separate CO_2 from a variety of gas streams [3]. Methyldiethanolamine (MDEA), monoethanolamine (MEA) and diethanolamine (DEA) are several examples of alkanolamines used in the CO_2 removal process. Due to low cost of solvent, high performance at low pressure and its rapid reaction rate with CO_2, aqueous MEA solution is still an interesting absorbent in industrial processes [4]. One of the most important advantages of MEA solution in comparison to other amines is its fast reaction rate with CO_2 due to carbamate formation, which reduces the size and height of a packed column [5].

The knowledge of the kinetics of CO_2 absorption into the solvent is crucial in the design of gas-liquid contactors for CO_2 capture units. In this regard, the experimental investigation on the reaction kinetics between MEA solution and CO_2 was carried out by several researchers using different gas-liquid contactors. For instance, Hikita et al. [6] used a rapid mixing method to evaluate the kinetics of reactive absorption of CO_2 in MEA solution at temperatures 278 to 308 K. They found that the reaction of CO_2 with MEA solution is first order with respect to MEA. Similarly, Penny and Ritter [7] measured CO_2 absorption rate in MEA solution at temperatures from 278 to 303 K and using stopped-flow method and proposed a kinetics constant for MEA. In another study, kinetics of CO_2 + MEA + H_2O system were examined by Horng and Li [8] at three temperatures of 303 K, 308 and 313 K, and using wetted wall

column. The authors used zwitterion mechanism to represent experimental data and reported the pseudo-first-order reaction rate constant. The overall reaction rate constant of CO_2 absorption into MEA solution was also evaluated by Luo et al. [9] using a string of discs contactor and at temperatures between 298 to 343 K. The authors developed a model to predict kinetics data based on the pseudo-first-order assumption.

Besides the reaction kinetics, the physical properties of a solvent such the density and viscosity play a crucial role in calculation of pumping cost, physical solubility and diffusivity of CO_2 [10]. Moreover, viscosity has a significant effect on the mass transfer performance. The solvents with high viscosity limit their application in the CO_2 capture process as well as increase mass transfer resistance. From these views, it is very important to measure the viscosity of MEA solution and investigate its effect on the mass transfer coefficient and CO_2 absorption flux. Recently, Bernhardsen et al. [11] conducted a study of CO_2 absorption into viscous MEA solution to investigate the effect of viscosity on the mass transfer coefficient in a membrane contactor. They found that decrease in the overall mass transfer coefficient with viscosity is independent of the solvent system.

It should be noted that CO_2-loaded absorbents are what really matters for industrial operating condition. A problem with the CO_2 loaded systems is that measuring the kinetics of these systems are complex and time-consuming. Moreover, reaction kinetics between CO_2 and loaded absorbents play an undeniably key role in acid gas treating processes through its influence on the size of the absorption tower. In this regard, the present work focuses on the effect of viscosity and MEA free concentration on mass transfer performance in 30 wt% MEA solution experimentally and theoretically. The viscosity of 30 wt% MEA solution is less than 2.5 mPa.s in a temperature range of 298.15 to 343.15 K. In order to evaluate the effect of high liquid viscosity on the mass transfer rate, a viscous solution is needed. The addition of the sugar or glycerol to the solution is one of the ways used in the literature to increase the liquid viscosity

[11]. The viscous MEA solution was prepared in this work by the addition of sugar due to its complete solubility, low price and Newtonian behavior in water. Therefore, the sugar was added at 3 to 20 wt% to achieve a viscous MEA solution with liquid viscosities of 2.8 to 8 mPa.s. The reaction kinetics of CO_2 absorption in unloaded and CO_2-loaded viscous MEA solutions were studied by measuring the overall mass transfer coefficient. The study aims to improve our understanding of the effect of viscosity on the mass transfer behavior of CO_2 absorption. Besides, the density and viscosity of unloaded and CO_2 loaded MEA + sugar solutions were measured and correlated using Redlich-Kister and modified Vogel-Tamman-Fulcher equations.

2. Background

2.1. Reaction mechanism

Caplow [12], Crooks and Donnellan [13] proposed zwitterion mechanism and termolecular mechanism, respectively, to describe reaction mechanisms between primary amine (RNH_2) solutions and CO_2. According to zwitterion mechanism, the carbamate is formed in a two steps reaction between MEA solution and CO_2, while termolecular mechanism presents a single step. These different reaction mechanisms lead to different kinetics models. In the first stage of zwitterion mechanism (Eq. 1), the zwitterion ion ($RNH_2^+COO^-$) as an intermediate is formed, then in the second stage (Eq. 2), $RNH_2^+COO^-$ undergoes deprotonation by a base B to form carbamate ($RNHCOO^-$). In these reactions, B could be an amine, CO_3^{2-}, HCO_3^-, H_2O or OH^- [14].

$$CO_2 + RNH_2 \leftrightarrow RNH_2^+COO^- \quad (1)$$

$$RNH_2^+COO^- + B \leftrightarrow RNHCOO^- + BH^+ \quad (2)$$

The reaction rate between MEA and CO_2, according to zwitterion mechanism can be described as follows:

$$R_{CO_2} = \frac{k_2[MEA][CO_2]}{1+\frac{k_{-1}}{\sum k_B[B]}} \quad (3)$$

when the zwitterion formation is the rate-determining step, the reaction rate is simplified as:

$$R_{CO_2} = k_2[CO_2][MEA] \quad (4)$$

On the other hand, the reaction rate takes the form Eq. (5), when the zwitterion deprotonation is a rate-determining step.

$$R_{CO_2} = \frac{[MEA][CO_2]}{\frac{1}{k_2}+\frac{1}{k_{MEA}[MEA]+k_{H_2O}[H_2O]+k_{OH}[OH^-]}} \quad (5)$$

Based on the termolecular mechanism, the reaction take place between MEA, CO_2 and base simultaneously as given in Eq. (6) [15]:

$$CO_2 + RNH_2 + B \leftrightarrow RNHCOO^- + BH^+ \quad (6)$$

The reaction rate described by termolecular mechanism was given by:

$$R_{CO_2} = \{k_{MEA}[MEA] + k_{H_2O}[H_2O]\}[CO_2][MEA] \quad (7)$$

In addition, CO_2 reacts with water, as in Eqs. (8-10):

$$H_2O + CO_2 \leftrightarrow H^+ + HCO_3^- \quad (8)$$

$$H_2O \leftrightarrow H^+ + OH^- \quad (9)$$

$$HCO_3^- \leftrightarrow H^+ + CO_3^{2-} \quad (10)$$

However, the overall contribution of the three reactions above for kinetics calculations is negligible in the presence of MEA [9]. Given the experimental difficulties associated with a correct rate law determination and in line with the most common approaches reported in the literature, a simple bimolecular kinetic law, Eq. (4), is assumed to be valid and adopted in the present work.

2.2. Mass transfer

The overall mass transfer coefficient (K_G) of CO_2 absorption in solution is expressed according to Eq. (11).

$$K_G = \frac{N_{CO_2}}{\Delta P_{CO_2}^{LM}} \quad (11)$$

where $\Delta P_{CO_2}^{LM}$ is the logarithmic mean of partial pressure of CO_2 at inlet and outlet of the gas-liquid contactor. In the general case of a system with CO_2 loaded solution, $\Delta P_{CO_2}^{LM}$ can be obtained as follows:

$$\Delta P_{CO_2}^{LM} = \frac{\left(P_{CO_2}^{in} - P_{CO_2}^{*,in}\right) - \left(P_{CO_2}^{out} - P_{CO_2}^{*,out}\right)}{\ln[(P_{CO_2}^{in} - P_{CO_2}^{*,in})/(P_{CO_2}^{out} - P_{CO_2}^{*,out})]} \quad (12)$$

where $P_{CO_2}^{in}$ and $P_{CO_2}^{out}$ are inlet and outlet partial pressure of CO_2, respectively, and $P_{CO_2}^{*,in}$ and $P_{CO_2}^{*,out}$ are equilibrium partial pressures. For the limiting case of an unloaded solution, the equilibrium partial pressures of CO_2 ($P_{CO_2}^{*,in}$ and $P_{CO_2}^{*,out}$) can be assumed to be zero. Therefore, the logarithmic mean of partial pressure of CO_2 can be determined using Eq. (13).

$$\Delta P_{CO_2}^{LM} = \frac{P_{CO_2}^{in} - P_{CO_2}^{out}}{\ln[P_{CO_2}^{in}/P_{CO_2}^{out}]} \quad (13)$$

According to two-film theory, K_G can be estimated by Eq. (14) (Luo et al. 2015):

$$\frac{1}{K_G} = \frac{1}{k_g} + \frac{H_{CO_2}}{E\, k_l} \quad (14)$$

with H_{CO_2} representing the Henry's constant and E representing the enhancement factor due the presence of the chemical reaction. For the string of discs contactor utilized in the present experimental investigation, previous works have determined the values of gas-film and liquid mass transfer coefficients as follows [16,17]:

$$k_g = 0.12 \left(\frac{D_{CO_2}}{d}\right) \left(\frac{\rho\, \upsilon\, d}{\mu}\right)^{0.79} \left(\frac{\mu}{\rho\, D_{CO_2}}\right)^{0.44} \quad (15)$$

$$k_l = 17.92\, D_{CO_2} \left(\frac{4\,\gamma}{\mu}\right) \left(\frac{\mu}{\rho\, D_{CO_2}}\right)^{0.5} \quad (16)$$

The enhancement factor (E) can be estimated from Hatta number (Ha) and infinite enhancement factor (E_∞). Equations of 17 and 18 give Hatta number and infinite enhancement factor when the bimolecular

reaction rate (Eq. 4) is assumed to describe the kinetics of the chemical reaction taking place between CO_2 and MEA.

$$\mathrm{Ha} = \frac{\sqrt{k_2\,[\mathrm{MEA}]\;D_{CO_2}}}{k_l} \tag{17}$$

$$E_\infty = 1 + \frac{D_{MEA}\,[\mathrm{MEA}]}{b\,D_{CO_2}\,C^i_{CO_2}} \tag{18}$$

In the present work care was taken so that all the experiments were carried out in the pseudo-first order regime, where $E_\infty \gg \mathrm{Ha}$, for which E=Ha, so that

$$K_G = \frac{1}{\frac{1}{k_g} + \frac{H_{CO_2}}{\sqrt{k_2\,[\mathrm{MEA}]\,D_{CO_2}}}} \tag{19}$$

For CO_2 loaded MEA solutions, it is assumed here that equation 3 is still the dominant one and its kinetic rate will depend this time on the concentration of free MEA present in the liquid bulk. To quantify how CO_2 loading affects concentration of the chemical species in the solution, thermodynamic equilibrium was assumed to prevail in the liquid bulk phase. The Kent-Eisenberg model was applied to determine the concentrations of $[CO_2]$, $[OH^-]$, $[CO_3^{2-}]$, $[RNH_3^+]$, $[RNHCOO^-]$, $[RNH_2]$, $[H^+]$ and $[HCO_3^-]$. The values of equilibrium constants (K_i) of chemical reactions between MEA aqueous solution and CO_2 were taken from the literature [18,19] (see **Table 1**) and expressed in the form:

$$\ln K_i = a_1 + \frac{a_2}{T} + a_3 \ln T \tag{20}$$

Table 1

MATLAB software was used to find the concentration of liquid-phase species (more details of modeling procedure, charge and material balance can be found in our previous work [4]. The profile of the concentration of liquid-phase species in the solution was plotted as a function of CO_2 loading in **Fig. 1** for the specific case of 30wt% MEA solution at 313.15 K.

Fig. 1

The concentration of carbamate reaches to a maximum value at CO_2 loading of 0.5, where MEA is nearly completely consumed. With further increasing CO_2 loading, carbamate concentration decreases due to the carbamate hydrolysis reaction, which leads to a rise in bicarbonate concentration. According to **Fig. 1**, in our interest range, for loading up to 0.5, free MEA concentration decreases practically linearly ($[\mathrm{MEA}]_{\mathrm{free}} = [\mathrm{MEA}]_{\mathrm{i}}(1-2\alpha)$). Therefore, for loaded solutions, replacing initial MEA concentration with free MEA concentration:

$$\mathrm{Ha} = \frac{\sqrt{\mathrm{k_2}\,[\mathrm{MEA}]\,(1-2\alpha)\,\mathrm{D_{CO_2}}}}{\mathrm{k_l}} \tag{21}$$

$$\mathrm{E_\infty} = 1 + \frac{\mathrm{D_{MEA}}\,[\mathrm{MEA}]\,(1-2\alpha)}{\mathrm{b}\,\mathrm{D_{CO_2}}\,\mathrm{C^i_{CO_2}}} \tag{22}$$

and K_G can then be estimated this time:

$$\mathrm{K_G} = \frac{1}{\frac{1}{\mathrm{k_g}} + \frac{\mathrm{H_{CO_2}}}{\sqrt{\mathrm{k_2}\,[\mathrm{MEA}]\,(1-2\alpha)\,\mathrm{D_{CO_2}}}}} \tag{23}$$

given that the pseudo-first-order regime was still attained in the experimental runs. When sugar is added to a MEA solution, its viscosity changes significantly (the change in density is on the other hand quite small) as well as the diffusivity and the physical solubility of CO_2. All the parameters described above are affected consequently. The working hypothesis here is that the same relationships can still be used by assuming the effect of the sugar on the physical parameters (viscosity, density, diffusivity, Henry constant) is correctly taken into account. In order to calculate diffusion coefficient of CO_2, Versteeg et al. [20] showed that the CO_2 diffusion in aqueous MEA solutions and water can be determined by Eq. (24) and Eq. (25), respectively.

$$\mathrm{D_{CO_2,solution}} = \mathrm{D_{CO_2,H_2O}} \times \left(\frac{\mu_{\mathrm{H_2O}}}{\mu_{\mathrm{solution}}}\right)^{0.8} \tag{24}$$

$$\mathrm{D_{CO_2,H_2O}} = 2.35 \times 10^{-6} \exp\left(\frac{-2119}{\mathrm{T}}\right) \tag{25}$$

Regarding solubility, Luo et al. [21] presented a correlation based on experimental data taken from Hartono et al. [22] to predict the physical solubility of CO_2 in 30 wt% MEA solution as a function of temperature and CO_2 loading as given in Eq. (26).

$$H_{CO_2} = \left(496.563 + 341697\frac{\alpha}{T}\right)\exp\left(1.69131\,\alpha^2 - \frac{1472.25}{T} - 128338\frac{\alpha}{T^2}\right) \quad (26)$$

This correlation was empirically modified in order to consider the effect of concentration of sugar on the physical solubility of CO_2 in the unloaded and CO_2 loaded MEA solutions.

$$H_{CO_2} = \left(H_{CO_2}\right)_{\text{Luo et al.}} \exp\left(f_1 W_2 + f_2 W_2^2\right) \quad (27)$$

Two adjustable parameters of f_1 and f_2 in Eq. (27) were found by fitting experimental data reported in the literature [11] for unloaded MEA + sugar solutions. A comparison between the predicted results for the physical solubility of CO_2 in MEA solutions using Eq. (27) and the experimental results measured by Bernhardsen et al. [11] was given in **Fig. 2**. The average absolute relative deviation (AARD) and parameters of f_1 and f_2 were found to be 2.3%, 0.986 and 0.079, respectively. The low value of AARD shows that the applied modified equation could be successfully used to represent the solubility of CO_2 in MEA solutions as a function of temperature, sugar concentration and CO_2 loading. **Table S5** presents the diffusivity and the physical solubility of CO_2 in MEA solutions.

Fig. 2

3. Chemicals and experimental procedure

3.1. Chemicals

In this work, sugar ($C_{12}H_{22}O_{11}$) was of a commercially available grade, while monoethanolamine (MEA, >98% purity) was obtained from Sigma-Aldrich and was used without further purification. Molecular structures of MEA and sugar were shown in **Fig. 3**. CO_2 and N_2 gases with purity >99.9% were prepared from AGA. The five blended solutions were used in this work, including 30 wt % MEA,

30 wt% MEA + 3 wt% sugar, 30 wt% MEA + 6 wt% sugar, 30 wt% MEA + 10 wt% sugar and 30 wt% MEA + 20 wt% sugar. A MS6002S Mettler Toledo balance with an uncertainty of ± 10^{-5} kg was used in this work in order to prepare the aqueous solutions of MEA. A variety of CO_2 loaded solutions from 0.1 to 0.4 (mol CO_2/mol MEA) were prepared by bubbling CO_2 from a gas cylinder in a glass bottle.

Fig. 3

3.2. Density and viscosity measurement

The density and viscosity measurements were carried out using an Anton Paar DMA 4500 density meter and an Anton Paar Lovis 2000 ME rolling-ball viscometer, respectively, at temperature ranging from 298.15 to 343 and at varying CO_2 loading values of 0.1 to 0.4 (mol CO_2/mol solvent). Before and after each run, the equipment was cleaned with acetone, and calibrated by measuring density and viscosity of pure water. Measurement of all solutions was conducted two times by the equipment and an average was reported in this work. The expanded uncertainties of density and viscosity measurements are 0.0027 g.cm^{-3} and 0.250 mPa.s, respectively, for unloaded solutions, and 0.0031 g.cm^{-3} and 0.253 mPa.s for CO_2-loaded solutions with a level of confidence equal to 95%. A detailed description of the equipment can be found in the literature [22,23].

3.3. The string of discs contactor

The reaction kinetics measurement of CO_2 absorption in unloaded and CO_2 loaded viscous MEA solutions was performed using the string of discs contactor. The details of the apparatus were given by Mamun et al. [24], and thus the main details will be summarized here. A schematic diagram of the string of discs contactor used in this work is presented in **Fig. 4**. As seen in this figure, the equipment consisted of two gas cylinders, a liquid pump, a gas blower, two mass flow controllers, a string of discs column, a CO_2 analyzer and several temperature indicators. The glass column with length of 64.5 cm as main part of this equipment has 43 discs with active mass transfer area equal to 2.19×10^{-2} m^2. Two mass flow

controllers with uncertainty less than 1% of measured flow were used to set the inlet flow rate of CO_2 and N_2. The CO_2 composition in the outlet gas stream was also analyzed using an IR CO_2 analyzer with an accuracy $\pm$0.01%, which was calibrated every day. In addition, the temperatures of inlet and outlet gas and liquid were controlled using several K-type thermocouples.

Briefly, in each run, the solution with desired concentration and loading was prepared and then fed into the column from the top by the liquid pump with a flow rate of 60 ml/min, while a mixture of CO_2 and N_2 with varying volume fraction of CO_2 between 0.2 and 5% enters from the bottom of column. Then, the system was allowed to come to a steady-state at desired temperature. A steady-state was attained when the CO_2 analyzer as well as gas and liquid temperatures, indicated constant values. In order to check the loading of the solution, a liquid sample was taken at the end of the experiment and analyzed for determining of CO_2 loading using Total Inorganic Carbon (TIC) analyzer. The absorption flux of CO_2 was obtained by a mass balance over the entire system. Finally, the overall mass transfer coefficient can be calculated using Eq. (11). The uncertainty of the K_G measurements is around 1%, as reported in Gondal et a. [25].

Fig. 4

4. Results and discussion

4.1. Density of the MEA (1) + sugar (2) + water (3) + CO_2 mixtures

In order to calculate the liquid mass transfer coefficient, values of density at different experimental conditions are required. Before measuring the density of MEA + H_2O + sugar + CO_2 system, the equipment and experimental data were validated by measuring densities of 30 wt% MEA and pure water in the temperature range of 298.15 to 343.15 K. The results from this work were compared to those reported by Bernhardsen et al. [11], Hartono et al. [22], Han et al. [26] and Spieweck et al. [27]. According to the results given in **Table S1** and **Fig. 5**, an excellent agreement between experimental data

obtained in this work and literature can be observed. The AARD between experimental density data measured in this work and those reported in the literature is about 0.08%.

Fig. 5

The densities of unloaded and CO_2 loaded MEA and MEA + sugar solutions were measured at temperatures from (298 to 343) K and the results were listed in **Table S2**. The effect of temperature and sugar concentration on the density of unloaded MEA and MEA + sugar is presented in **Fig. 6**. It can clearly be seen in this figure that the density of solution decreases with a rise in temperature from 298.15 to 343.15 K. As expected, density increased with increasing sugar concentration at the constant temperature. A similar trend was observed for CO_2 loaded solutions.

Fig. 6

The density of CO_2 loaded MEA and MEA + sugar solutions was also investigated by varying the loading of solution from 0 to 0.4 (mol CO_2/mol solvent). The density of MEA and MEA + sugar solutions at different CO_2 loading values was plotted in **Fig. 7** and **Fig. 8**, respectively. According to these figures, the increase of CO_2 loading leads to the increase in density of solution. In addition, it was found that the CO_2 loading has a significant effect on density of solution, while temperature showed a small effect.

Fig. 7

Fig. 8

The Redlich-Kister equation was applied in this work to fit the experimental density data. This technique was frequently used in the literature [28-30] to represent the excess properties, and can be expressed as:

$$V^E = V_m - \sum_i x_i V_i \quad (28)$$

Where V^E, x_i and V_i are excess molar volume, mole fraction and molar volume of pure component, respectively. The molar volume of mixture (V_m) is calculated using Eq. (29) and knowing of values of experimental density data of CO_2-free solution ($\rho_{\alpha=0}$).

$$V_m = \frac{\sum_i x_i M_i}{\rho_{\alpha=0}} \quad (29)$$

The excess molar volume of a binary system can be defined by the following equation:

$$V_{ij}^E = x_i x_j \sum_{k=0}^{n} A_k (x_i - x_j)^k \quad (30)$$

There are several different forms for calculation of adjustable parameter (A_k) in Eq. (31) as follows:

$$A_k = \frac{a_k}{T};\ A_k = a_k + b_k T; A_k = a_k + b_k T + c_k T^2 \quad (31)$$

To reduce the numbers of parameters, a_k/T was used in this work for A_k. Eq. (32) can be used in order to calculate of the excess molar volume for ternary systems.

$$V^E = V_{12}^E + V_{13}^E + V_{23}^E \quad (32)$$

The binary parameters of Redlich-Kister equation were determined by regression of experimental data and the results were provided in **Table 2**.

Table 2

The density of unloaded MEA and MEA + sugar solutions was calculated according to the Redlich-Kister equation and values of fitting parameters. A comparison between the experimental density data and modeling results is given in **Figs. 6-8**. There is a very good agreement between experimental density data and the model results with an AARD equal to 0.1%. For correlating of the density of CO_2 loaded solutions, the effect of CO_2 loading was taken into account by adding an item to Redlich-Kister equation as follows:

$$\frac{\rho_{\alpha\neq 0}}{\rho_{\alpha=0}} = (1 + \alpha \times (b_1 + b_2 \times w_2)) \quad (33)$$

where α and w_2 are CO_2 loading and mass fraction of sugar, respectively. In the above equation, b_1 and b_2 are adjustable parameters that were determined by fitting again with experimental data. The values of b_1 and b_2 were found to be 0.244 and 0.0017, respectively. The predicted values of density by Eq. (33) for CO_2 loaded solutions were shown as solid lines in **Fig. 6** and **Fig. 8**. It can be observed that predicted results agree well with experimental data. In addition, AARDs value was found to be 0.39% for loaded

solutions. The parity plot between experimental density data and model results for unloaded and CO_2 loading MEA and viscous MEA was presented in **Fig. 9**.

Fig. 9

4.2. Viscosity of the MEA (1) + sugar (2) + water (3) + CO_2 mixtures

The viscosity data of solvent at different experimental conditions are important in order to determine CO_2 diffusivity, mass transfer coefficient and kinetics modeling. Similar to density procedure, a comparison between the viscosity of 30wt% MEA solution measured in this work and values reported in the literature [11,22,31] was made for validation purposes. As can be observed in **Table S3** and **Fig. 10**, the results determined in this work and viscosity values in the literature are in good agreement with an AARD equal to 1.94%.

Fig. 10

As mentioned before, sugar with concentration of 3 to 20 wt% was added to 30 wt% MEA solution to prepare a viscous solution. The viscosity of unloaded and CO_2 loaded MEA and MEA + sugar in the temperature range 298 to 343 K was measured and the results were summarized in **Table S4**. The effect of sugar concentration on the viscosity of the solution is shown in **Fig. 11**. A seen from this figure, the viscosity increases significantly when sugar concertation increases from 10 to 20 wt%.

Fig. 11

In order to investigate the effect of CO_2 loading on viscosity, the viscosity of MEA and MEA + sugar solutions at CO_2 loading range of 0 to 0.4 was measured and the results were plotted as a function of temperature in **Fig. 12** and **Fig. 13**, respectively. The experimental results indicate that the viscosity increases as CO_2 loading increases and decreases with rise in temperature. In other words, CO_2 absorption in the solvent leads to a viscous solution which is not favorable for gas absorption industrial application. The reduction of viscosity with temperature can be explained by the fact that at high temperature, the

kinetic energy between molecules increases, which lead to decrease viscosity. It was also observed that the effect of temperature on viscosity at CO_2 loaded solutions is greater than that at unloaded solutions.

Fig. 12

Fig. 13

The Vogel-Fulcher-Tammann (VFT) equation was used by many researchers [32-34] to describe the viscosity of solutions. A modified version of this equation was applied in this work to correlate experimental viscosity data as a function of temperature, sugar concentration and CO_2 loading as follow:

$$\frac{\mu_{\alpha\neq0}}{\mu_{\alpha=0}} = \exp\left[\alpha\left(b_4 + b_5\, W_2 + b_6\, W_2^2\right)\right] \quad (34)$$

$$\mu_{\alpha=0} = \exp\left(B_1 + \frac{B_2}{T}\right) \quad (35)$$

$$B_1 = b_{11} + b_{12}\, W_2 + b_{13}\, W_2^2 \quad (36)$$

$$B_2 = b_{21} + b_{22}\, W_2 + b_{23}\, W_2^2 \quad (37)$$

where W_2 and b_i are sugar mass fraction and adjustable parameters, respectively. The values for the adjustable parameters were listed in **Table 3**.

Table 3

The predicted viscosity from VFT equation along with experimental data for unloaded and CO_2 loaded solutions were presented in **Figs. 11-13**. It can be concluded that the proposed model in this work is able to describe the viscosity of a solution with a good agreement. The AARD values between the experimental data and calculated viscosities were found to be 1.89% and 4.22% for unloaded and loaded solutions, respectively. The comparison between viscosity experimental data and model results was given in **Fig. 14** in the form of a parity plot.

Fig. 14

4.3. The overall mass transfer coefficient

4.3.1. Unloaded system

The K_G of CO_2 absorption in aqueous 30 wt% unloaded MEA solution at a temperature range of 298 to 343 K were first measured to verify the reliability of the string of disc apparatus. The results were compared with those published in the literature [11,21] for the same experimental setup as presented in **Fig. 15**. According to this figure, K_G data measured in this work are in an excellent agreement with those published in the literature with AARD of 4.29%.

Fig. 15

The experimental second-order reaction rate constant (k_2) obtained in this work for 30 wt% unloaded MEA solution was fitted to Arrhenius expression. Eq. (38) presents temperature dependence of reaction rate constant obtained in this work.

$$k_2 = 1.72 \times 10^{11} \exp\left(\frac{-4915.5}{T}\right) \quad (38)$$

According to Eq. (38), the activation energy was found to be 40.86 kJ/mol which is in good agreement with those reported by Versteeg et al. (44.9 kJ/mol), Hikita et al. (41.2 kJ/mol), Penny et al. (42.2 kJ/mol) and Horng et al. (44.7 kJ/mol). **Fig. 16** shows a comparison between predicted reaction rate constant (k_2) using model presented in this work and those of Versteeg et al. [35], Hikita et al. [6], Penny et al. [7], Horng et al. [8], Luo et al. [21], Liao et al. [36] and Alper [37]. As can be seen from **Fig. 16**, k_2 reported in this work was found to be in good agreement with those of Luo et al. and Liao et al. However, a deviation can be observed with other models. This deviation could be due to the different experimental conditions and measurement techniques. For example, Horng et al. and Penny et al. proposed their models based on MEA concentration less than 0.5 kmol/m^3 and temperatures up to 313 K, which is much lower than the experimental condition used in this work.

Fig. 16

The k_2 values determined earlier, Eq. (38), for unloaded MEA solution were inserted in Eq. (19) to model behavior of K_G of CO_2 absorption in unloaded MEA solution as a function of temperature. The performance of the kinetics model for modeling the experimental K_G data for unloaded MEA solution (red line) was presented in **Fig. 17** (uppermost point). In this figure, the solid lines are modeling results and the points are the experimental K_G data. As expected, a very good agreement can be observed.

4.3.2. CO_2 loaded system

To investigate the effect of MEA free concentration on mass transfer performance, the CO_2 loading of the solution was changed from 0 (unloaded) to 0.4 mol CO_2/mol solvent. K_G measurement for 30 wt% CO_2 loaded MEA solutions were carried out at temperatures from 298 to 343 K, and the results were tabulated in **Table S5**. K_G of CO_2 absorption in MEA solution at different CO_2 loadings as a function of temperature was also plotted in **Fig. 17**. It was found that K_G decreases with increasing CO_2 loading of MEA solution. When CO_2 loading of solution increases, not only viscosity of solution increases but also the free concentration of MEA reduces in the solution. Therefore, less MEA ions are available in solution to react with CO_2, which leads to decrease enhancement factor and overall mass transfer coefficient. Moreover, it can clearly be seen from **Fig. 17** that K_G increases as the temperature increases from 298 to 343 K which can be explained due to a corresponding decrease of the viscosity of the solution and increase reaction kinetics with temperature. To model the K_G of CO_2 absorption in CO_2 loaded MEA solutions, the same values for k_2 was used. In other words, Eq. (38) which was obtained based on unloaded MEA solution was applied and inserted in Eq. (23) to predict mass transfer behavior of CO_2 absorption in CO_2 loaded MEA solution. As can be seen in **Fig. 17**, there is a good agreement between experimental data and modeling results which means second order reate conctant for unloaded MEA can be used to predict CO_2 loaded MEA system.

Fig. 17

The experimental second order rate constants determined in this work for unloaded and CO_2 loaded 30 wt% MEA solution as a function of temperature were given in **Fig. 18**. From the data obtained, it can be observed that CO_2 loading has negligible effect on reaction rate constant, as assumed in the first part of this work. The same results were observed in MEA + sugar systems.

Fig. 18

4.3.3. Viscous system

It is of interest to understand how high viscosity affects the mass transfer performance of solvent. In order to study the influence of viscosity on the mass transfer coefficient, sugar with different concentrations was added to MEA to increase solution viscosity. The experiments were conducted over the sugar concentration range of 3-20 wt%. The effect of viscosity on K_G of unloaded MEA solution was presented in **Fig. 19**. The K_G of viscous MEA solutions at different CO_2 loading values was also measured and the results were given in **Fig. 20**.

Fig. 19

Fig. 20

The same procedure was made to model CO_2 mass transfer in viscous MEA solution as a function of temperature and CO_2 loading. From **Fig. 19** and **Fig. 20**, it may be concluded that the model developed in this work based on bimolecular kinetic rate law is able to predict mass transfer experimental data in unloaded and CO_2 loaded MEA and viscous MEA solutions well with AARD equal to 6.12%. The parity plots of experimental mass transfer data and modeling results is given in **Fig. 21**. The experimental values of second-order reaction rate constant for unloaded and CO_2 loaded viscous MEA systems were calculated and the results for unloaded viscous MEA were given in **Fig. 22**. It can be observed from this figure that as expected, the viscosity has no effect on the second-order rate constant over the whole temperature range from 298 to 343 K. However, 30 wt% MEA + 20 wt% sugar shows a bit deviation.

This data scattering can be due to high viscosity and less CO_2 driving force in this system, which increases experimental uncertainty in the reaction kinetics investigation. Therefore, the assumption that the rate constant for unloaded MEA can be used to predict unloaded and loaded viscous MEA is valid. Values of infinite enhancement factor and Hatta number were determined using Eq. (21) and Eq. (22), and the results were listed in **Table S5**. It was observed that at all temperatures and CO_2 loadings, the assumption of the pseudo-first-order reaction regime is valid.

Fig. 21

Fig. 22

To have a better understanding of effect of MEA free concentration on mass transfer behavior, mass transfer coefficient of three different systems which have same viscosity was measured. According to **Fig. 23**, at the same viscosity, the solution with more active free MEA ions has higher K_G in comparison with the other two systems. Furthermore, this figure indicates how CO_2 loading can affect and decrease mass transfer coefficient of a solvent in the capture plant. For example, at a temperature of around 313 K, K_G decreases significantly from 21.2×10^{-4} to 6.9×10^{-4} (mol/m^2.kPa.s) when loading of MEA is changed from unloaded condition to CO_2 loading equal to 0.4 (mol CO_2/mol solvent). The effect of MEA free concentration on mass transfer at different viscosity values and 313.15 K was plotted in **Fig. 24**. From this figure, it was concluded that the negative effect of MEA free concentration on K_G is greater at low viscosities. It was also found that K_G is most sensitive to increasing CO_2 loading. Therefore, solvent-free concentration is an important parameter and should be considered in the absorption process.

Fig. 23

Fig. 24

Fig. 25 shows the performance of two different systems with the same viscosity and same MEA free concentration in terms of K_G values. To make a comparison, solutions of 30wt% MEA + 3.4wt% sugar at CO_2 loading of 0.25 and unloaded 15wt% MEA + 26wt% sugar were prepared. The experimental K_G

data and modeling results of these two systems as a function of temperature were presented in **Fig. 25**. As is illustrated, 30wt% MEA + 3.4wt% sugar with loading of 0.25 and unloaded 15wt% MEA + 26wt% sugar solutions have approximately the same overall mass transfer coefficients. In rigorous kinetic models based on penetration theory, the diffusivity of the ionic species, like carbamate, as well as free MEA are modeled to be dependent on solution viscosity and temperature [38]. However, the different ionic species are likely to have different diffusivities [39]. The overall mass transfer coefficient, in **Fig. 25**, is equally high for cases where the viscosity is increased by adding sugar and in the cases where the viscosity is increased by increasing loading leading/ionic species in the solution. Thus, the new data show that by measuring absorption kinetics of unloaded solution, one can predict the absorption rates of loaded solutions as long as one knows the viscosity of the loaded solution and has a thermodynamic model able to predict the physical solubility CO_2, speciation and partial pressure of CO_2 (for driving for calculations). The K_G values of unloaded MEA solutions as a function of viscosity at different temperatures was given in **Fig. 26**. It can be observed that as viscosity increases, K_G reduction with viscosity is greater at high temperatures compared to low temperatures. The same results were observed at CO_2 loaded systems. Moreover, it was concluded that the viscosity effect on K_G is less than the effect of amine free concentration. This is an interesting result since it indicates that the decrease in absorption with increased loading is purely due to a free concentration effect.

Fig. 25

Fig. 26

5. Conclusion

A string of disc contactor was used in this work to study the kinetics of reaction between CO_2 and loaded viscous MEA solution. The experimental results revealed that K_G enhanced with increasing temperature while decreases as CO_2 loading and viscosity increase. The amine free concentration

exhibited a significant effect on mass transfer while viscosity had little effect which shows that the decrease in absorption with loading is purely due to a free concentration effect. The K_G was found to decreases rapidly with loading at low viscosities, but this impact is less significant at higher viscosities. It was also concluded that K_G decreases faster with viscosity when the temperature is higher. It was observed that CO_2 loading and viscosity effect on the second order rate constant is negligible. A new kinetic model based on the pseudo first order regime was developed to describe CO_2 absorption behavior in the solution. The activation energy and second order reaction rate constant were found to be 40.86 kJ/mol and $k_2 = 1.72 \times 10^{11} \exp(-4915.5/T)$, respectively. The developed model showed a good ability to predict K_G for CO_2 + MEA, CO_2 + loaded MEA, CO_2 + viscous MEA and CO_2 + loaded viscous MEA systems at a wide range of temperature with AARD of 6.12%. Furthermore, density and viscosity of MEA solution were successfully correlated with excellent accuracy. The results showed that density and viscosity decreased with the temperature and increased with the rise in CO_2 loading.

Nomenclature

MEA	Monoethanolamine
MDEA	Methyldiethanolamine
DEA	Diethanolamine
k_2	Reaction rate constant (m_3/mol.s)
K_G	Overall mass transfer coefficient (mol/m^2.kPa.s)
k_g	Gas mass transfer coefficient (mol/m^2.kPa.s)
k_l	Liquid mass transfer coefficient (mol/m^2.kPa.s)
E	Enhancement factor
Ha	Hatta number
$\mathbf{E}_\infty$	Infinite enhancement factor
μ	Viscosity (mPa.s)
P	Density (g/cm^3)

$\mathbf{D_{CO_2}}$	Diffusivity of CO_2 (m^2/s)
$\mathbf{H_{CO_2}}$	Physical solubility of CO_2 ($kPa.m^3/kmol$)
$\mathbf{P^b_{CO_2}}$	CO_2 partial pressure in gas phase
$\mathbf{P^i_{CO_2}}$	CO_2 partial pressure in interface
$\mathbf{C^i_{CO_2}}$	CO_2 concentration in interface
$\mathbf{C^b_{CO_2}}$	CO_2 concentration in liquid phase
$\mathbf{\Delta P^{LM}_{CO_2}}$	logarithmic mean of CO_2 partial pressure
k_{ov}	Overall reaction rate constant (1/s)
b	Stoichiometric coefficient of CO_2
$\mathbf{V^E}$	Excess molar volume
$\mathbf{V_m}$	Molar volume
$\mathbf{x_i}$	Mole fraction
$\mathbf{M_i}$	Molecular weight
$\boldsymbol{\alpha}$	CO_2 loading
W_2	Sugar mass fraction
b_{ij}	Adjustable parameters

Appendix A. Supporting information

See Tables S1-S5.

References

[1] S. Garg, Gh. Murshid, F. Mjalli, A. Ali, W. Ahmad, Experimental and correlation study of selected physical properties of aqueous blends of potassium sarcosinate and 2-piperidineethanol as a solvent for CO_2 capture. Chem. Eng. Res. Des. 118 (2017) 121-130.

[2] G. Astarita, D. Savage, A. Bisio, Gas treating with chemical solvents; John Wiley & Sons: New York, 1983.

[3] I. Sreedhar, T. Nahar, A. Venugopal, B. Srinivas, Carbon capture by absorption-path covered and ahead, Renew. Sust. Energ. Rev. 76 (2017) 1080-1107.

[4] R. Ramezani, S. Mazinani, R. Di Felice, A comprehensive kinetic and thermodynamic study of CO_2 absorption in blends of monoethanolamine and potassium lysinate: Experimental and modeling. Chem. Eng. Sci. 206 (2019) 187-202.

[5] K. Fu, G. Chen, Zh. Liang, T. Sema, R. Idem, P. Tontiwachwuthikul, Analysis of mass transfer performance of monoethanolamine-based CO_2 absorption in a packed column using artificial neural networks. Ind. Eng. Chem. Res. 53 (2014) 4413-4423.

[6] H. Hikita, S. Asai, H. Ishikawa, M. Honda, The kinetics of reaction of carbon dioxide with monoethanolamine, diethanolamine and triethanolamine by a rapid mixing method. Chem. Eng. J. 13 (1977) 7-12.

[7] D. Penny, T. Ritter, Kinetic study of reaction between carbon dioxide and primary amines. Journal of Chemical Society Faraday Transactions. 79 (1983) 2103-2109.

[8] S. Horng, M. Li, Kinetics of absorption of carbon dioxide into aqueous solutions of monoethanolamine + triethanolamine. Ind. Eng. Chem. Res. 41 (2002) 257-266.

[9] X. Luo, A. Hartono, H. Svendsen, Comparative kinetics of carbon dioxide absorption in unloaded aqueous monoethanolamine solutions using wetted wall and string of discs columns, Chem. Eng. Sci. 82 (2012) 31-43.

[10] Z. Idris, J. Chen, D. Eimer, Densities of unloaded and CO_2 loaded 3-dimethylamino-1-propanol at temperatures (293.15 to 343.15) K, J. Chem. Thermodynamics 97 (2016) 282-289.

[11] I. M. Bernhardsen, L. Ansaloni, H. Betten, L. Deng, H. K. Knuutila, Effect of liquid viscosity on the performance of a non-porous membrane contactor for CO_2 capture, Sep. Purif. Technol. 222 (2019) 188-201.

[12] M. Caplow, Kinetics of carbamate formation and breakdown. J. Am. Chem. Soc. 90 (1968) 6795-6803.

[13] J. Crooks, J. Donnellan, Kinetics and mechanism of the reaction between carbon dioxide and amines in aqueous solution, J. Chem. Soc. Perkin Trans. 2 (1989) 331-333.

[14] N. Ramachandran, A. Aboudheir, R. Idem, P. Tontiwachwuthikul, Kinetics of the absorption of CO_2 into mixed aqueous loaded solutions of monoethanolamine and methyldiethanolamine, Ind. Eng. Chem. Res. 45 (2006) 2608-2616.

[15] Sh. Chen, X. Han, X. Sun, X. Luo, Zh. Liang, The comparative kinetics study of CO_2 absorption into non-aqueous DEEA/MEA and DMEA/MEA blended systems solution by using stopped-flow Technique, Chem. Eng. J. 386 (2020) 121295.

[16] S. Ma'mun, V. Dindore, H.F. Svendsen, Kinetics of the reaction of carbon dioxide with aqueous solutions of 2-((2-aminoethyl)amino)ethanol, Ind. Eng. Chem. Res. 46 (2007) 385-394.

[17] E. Stephens, G. Morris, Determination of liquid-film absorption coefficients. A new type of column and its application to problems of absorption in presence of chemical reaction, Chem. Eng. Prog. 47 (1951) 232-42.

[18] M. Wagner, I. Harbou, J. Kim, I. Ermatchkova, G. Maurer, Solubility of carbon dioxide in aqueous solutions of monoethanolamine in the low and high gas loading regions, J. Chem. Eng. Data 58 (2013) 883-895.

[19] M. Haji-Sulaiman, M.K. Aroua, A. Benamor, Analysis of equilibrium data of CO_2 in aqueous solutions of diethanolamine (DEA), methyldiethanolamine (MDEA) and their mixtures using the modified Kent-Eisenberg model, Chem. Eng. Res. Des. 76 (1998) 961-968.

[20] G. F. Versteeg, W.P. Van Swaiij, Solubility and diffusivity of acid gases (carbon dioxide and nitrous oxide) in aqueous alkanolamine solutions, J. Chem. Eng. Data 33 (1988) 29-34.

[21] X. Luo, A. Hartono, S. Hussain, H. F. Svendsen, Mass transfer and kinetics of carbon dioxide absorption into loaded aqueous monoethanolamine solutions, Chem. Eng. Sci. 123 (2015) 57-69.

[22] A. Hartono, E. Orji Mba, H. F. Svendsen, Physical properties of partially CO_2 loaded aqueous monoethanolamine (MEA), J. Chem. Eng. Data 59 (2014) 1808-1816.

[23] D. Pinto, J. Monteiro, B. Johnsen, H. Svendsen, H. Knuutila, Density measurements and modelling of loaded and unloaded aqueous solutions of MDEA (N-methyldiethanolamine), DMEA (N,N-dimethylethanolamine), DEEA (diethylethanolamine) and MAPA (N-methyl-1,3-diaminopropane), Int. J. Greenh. Gas Con. 25 (2014) 173-185.

[24] Sh. Ma'mun, V. Dindore, H. F. Svendsen, Kinetics of the reaction of carbon dioxide with aqueous solutions of 2-((2-aminoethyl)amino)ethanol, Ind. Eng. Chem. Res. 46 (2007) 385-394.

[25] Sh. Gondal, N. Asif, H. F. Svendsen, H. Knuutila, Kinetics of the absorption of carbon dioxide into aqueous hydroxides of lithium, sodium and potassium and blends of hydroxides and carbonates, Chem. Eng. Sci. 123 (2015)487-499.

[26] J. Han, J. Jin, D. Eimer, M. Melaaen, Density of water (1) + monoethanolamine (2) + CO_2 (3) from (298.15 to 413.15) K and surface tension of water (1) + monoethanolamine (2) from (303.15 to 333.15) K. J. Chem. Eng. Data 57 (2012) 1095-1103.

[27] F. Spieweck, H. Bettin, Review: solid and liquid density determination/ubersicht: bestimmung der dichte von festkorpern und flussigkeiten. TM, Tech. Mess. 59 (1992) 285-292.

[28] X. Shi, Ch. Li, H. Guo, Sh. Shen, density, viscosity, and excess properties of binary mixtures of 2-(methylamino)ethanol with 2-methoxyethanol, 2-ethoxyethanol, and 2-butoxyethanol from 293.15 to 353.15 K, J. Chem. Eng. Data 64 (2019) 3960-3970.

[29] X. Luo, L. Su, H. Gao, X. Wu, R. Idem, P. Tontiwachwuthikul, Zh. Liang, density, viscosity, and N_2O solubility of aqueous 2-(methylamino)ethanol solution, J. Chem. Eng. Data 62 (2017) 129-140.

[30] H. Guo, L. Hui, Sh. Shen, Monoethanolamine + 2-methoxyethanol mixtures for CO_2 capture: density, viscosity and CO_2 solubility, J. Chem. Thermodynamics 132 (2019) 155-163.

[31] T. Amundsen, L. Øi, D. Eimer, Density and viscosity of monoethanolamine + water + carbon dioxide from (25 to 80) °C, J. Chem. Eng. Data 54 (2009) 3096-3100.

[32] G. Murshid, W. Ahmad Butt, S. Garg, Investigation of thermophysical properties for aqueous blends of sarcosine with 1-(2-aminoethyl) piperazine and diethylenetriamine as solvents for CO_2 absorption, J. Mol. Liq. 278 (2019) 584-591.

[33] S. Garg, A. Shariff, M. Shaikh, B. Lal, A. Aftab, N. Faiqa, Selected physical properties of aqueous potassium salt of l-phenylalanine as a solvent for CO_2 capture, Chem. Eng. Res. Des. 113 (2016) 169-181.

[34] A. Garcia, R. Leron, A. Soriano, M. Li, Thermophysical property characterization of aqueous amino acid salt solutions containing a-aminobutyric acid, J. Chem. Thermodynamics 81 (2015) 136-142.

[35] G. Versteeg, L. Dijck, P. Swaaij, On the kinetics between CO_2 and alkanolamines both in aqueous and non-aqueous solutions, An overview, Chem. Eng. Commun. 144 (1996) 113-158.

[36] Ch. Liao, M. Li, Kinetics of absorption of carbon dioxide into aqueous solutions of monoethanolamine + N-methyldiethanolamine, Chem. Eng. Sci. 57 (2002) 4569-4582.

[37] E. Alper, Reaction mechanism and kinetics of aqueous solutions of 2-amino-2-methyl-1-propanol and carbon dioxide, Ind. Eng. Chem. Res. 29 (1990) 1725-1728.

[38] A. Aboudheir, P. Tontiwachwuthikul, A. Chakma, R. Idem, Kinetics of the reactive absorption of carbon dioxide in high CO_2-loaded, concentrated aqueous monoethanolamine solutions, Chem. Eng. Sci. 58 (2003) 5195-5210.

[39] S. M. Melnikov, M. Stein, The effect of CO_2 loading on alkanolamine absorbents in aqueous solutions, Phys. Chem. Chem. Phys. 21 (2019) 18386-18392.

Table 1 The equilibrium constants of chemical reactions between CO_2 and MEA solution

K_i (kmol/m^3)	a_1	a_2	a_3	Ref.[18,19]
$\mathbf{K_1} = [\mathbf{RNH_2}][\mathbf{HCO_3^-}]/[\mathbf{RNHCOO^-}]$	6.69425	-3090.83	0	Wagner et al.
$\mathbf{K_2} = [\mathbf{RNH_2}][\mathbf{H^+}]/[\mathbf{RNH_3^+}]$	-3.3636	-5851.11	0	Wagner et al.
$\mathbf{K_3} = [\mathbf{H^+}][\mathbf{HCO_3^-}]/[\mathbf{CO_2}]$	235.485	-12092.1	-36.7816	Haji-Sulaiman et al.
$\mathbf{K_4} = [\mathbf{H^+}][\mathbf{OH^-}]$	140.932	-13445.9	22.4773	Haji-Sulaiman et al.
$\mathbf{K_5} = [\mathbf{H^+}][\mathbf{CO_3^{2-}}]/[\mathbf{HCO_3^-}]$	220.067	-12431.7	-35.4819	Haji-Sulaiman et al.

Table 2 Fitted binary parameters in Eq. (30)

	Binary pair		
Parameter	**MEA-sugar**	**MEA-H_2O**	**Sugar-H_2O**
$\mathbf{a_0}$	-145.475	-996.147	-826.234
$\mathbf{a_1}$	-16.8998	54.1617	374.126
$\mathbf{a_2}$	-1.33796	628.959	-205.547

Table 3 Fitted parameters of the Vogel-Fulcher-Tammann (VFT) equation

	$\mathbf{b_{11}}$	$\mathbf{b_{12}}$	$\mathbf{b_{13}}$	$\mathbf{b_{21}}$	$\mathbf{b_{22}}$	$\mathbf{b_{23}}$	$\mathbf{b_4}$	$\mathbf{b_5}$	$\mathbf{b_6}$
Parameters	-6.929	-4.059	7.446	2332.42	2458.96	89.3419	1.028	3.551	-0.518

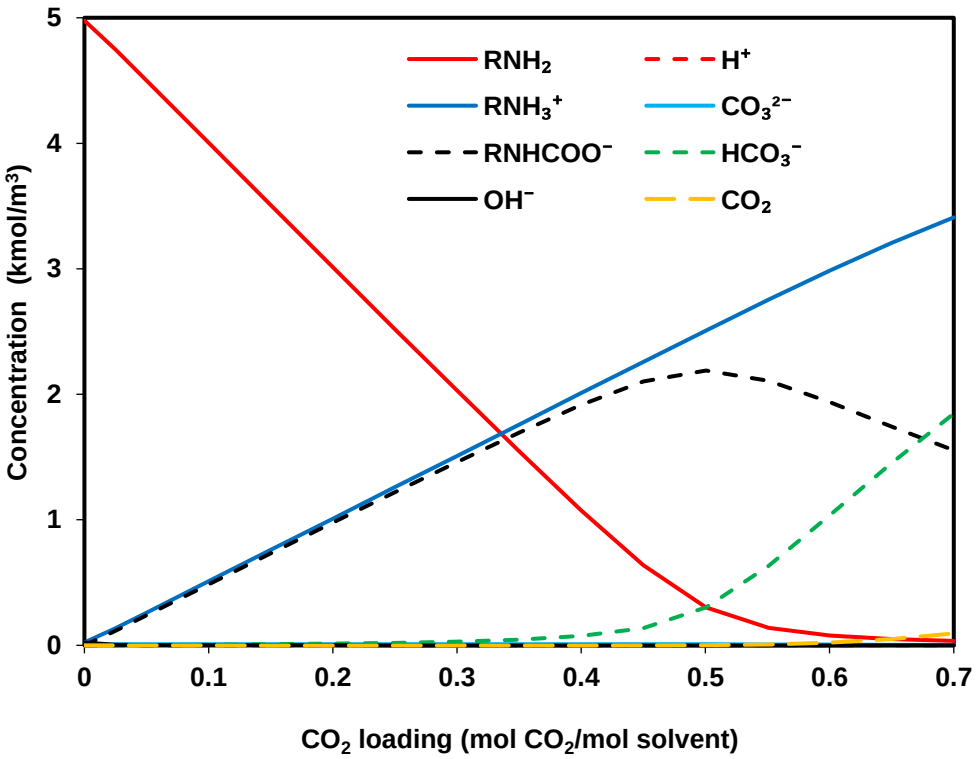

Fig. 1 Particle speciation as calculated from equilibrium for a 30% MEA solution at 313.15 K

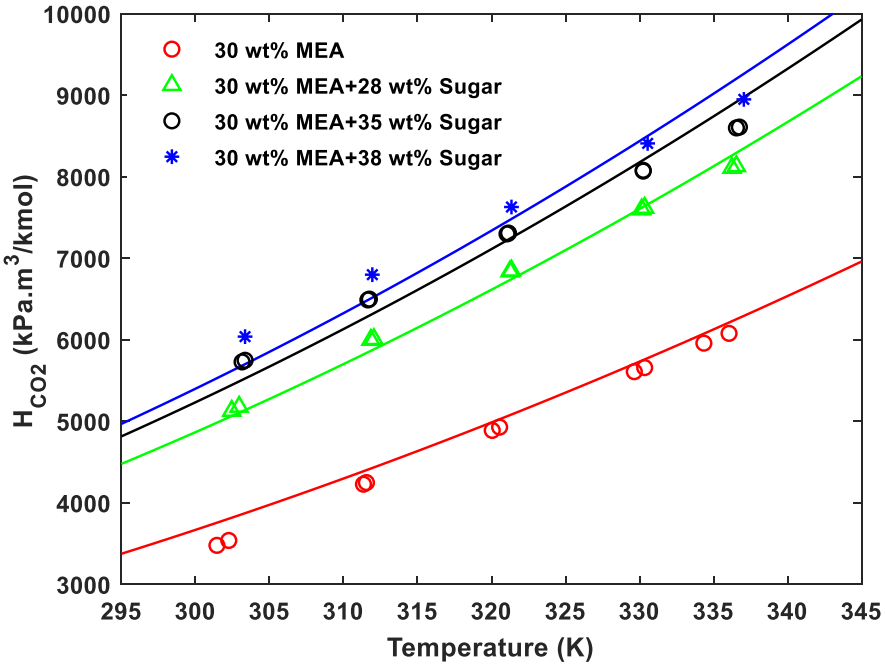

Fig. 2 The physical solubility of CO_2 in MEA and MEA + sugar solutions. Points: experimental data from Bernhardsen et al. [11], Lines: calculated from Eq. (27).

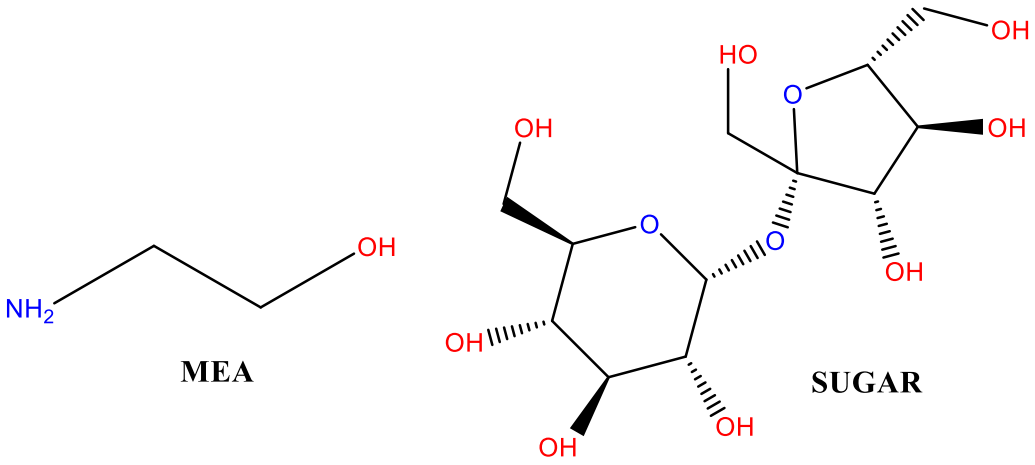

Fig. 3 Molecular structure of MEA and sugar

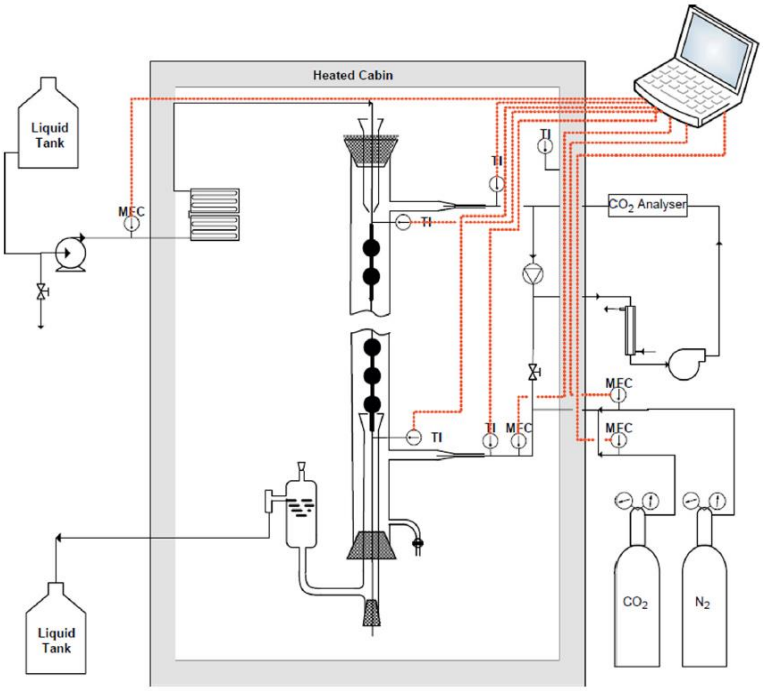

Fig. 4 Schematic diagram of the string of discs contactor. The figure taken from Luo et al. (2015)

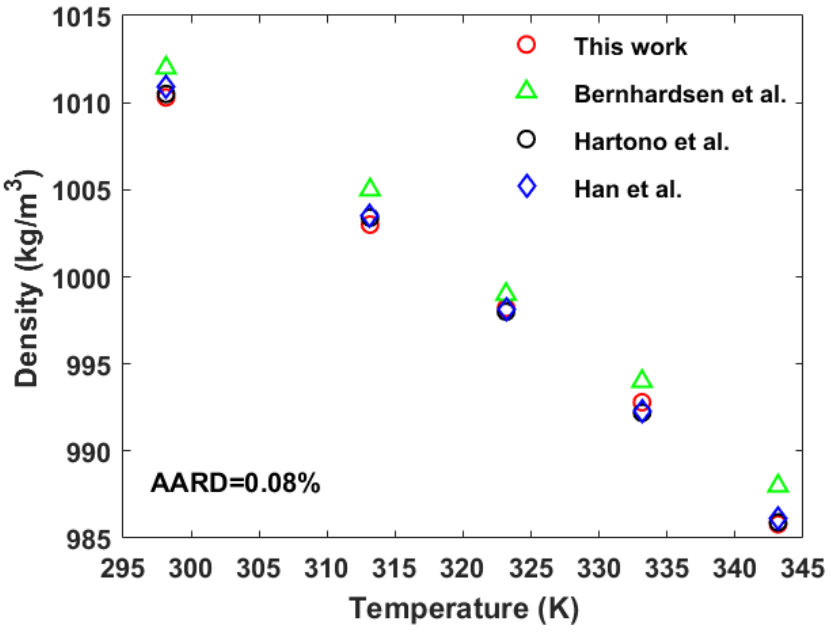

Fig. 5 Density values of 30 wt% MEA measured in this work and reported in the literature

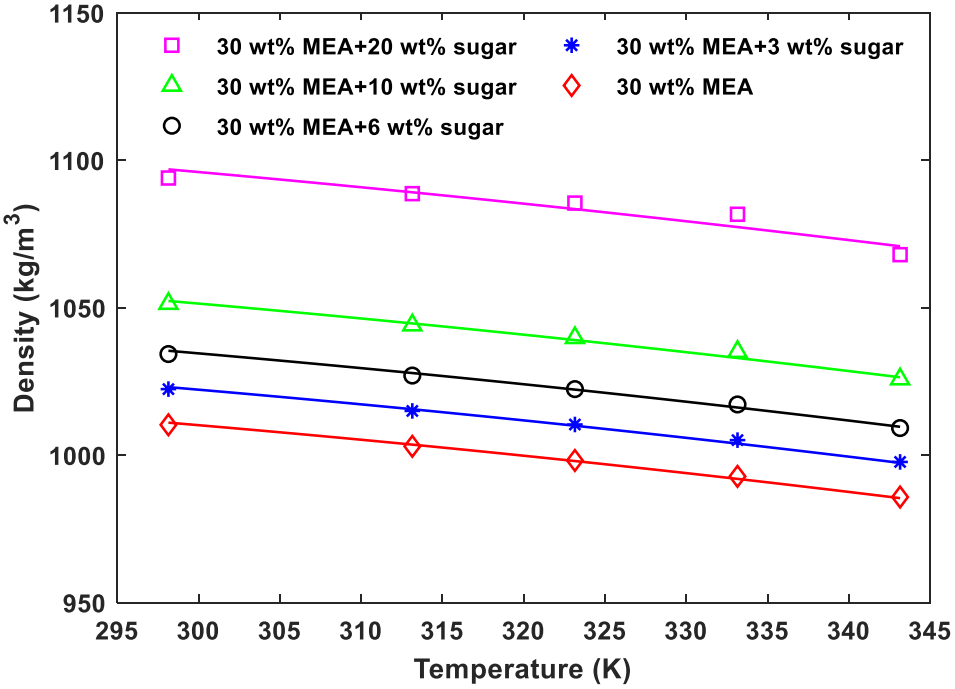

Fig. 6 Density of unloaded MEA and MEA + sugar solutions versus temperature. Points: experimental data, Lines: calculated from Eq. (33).

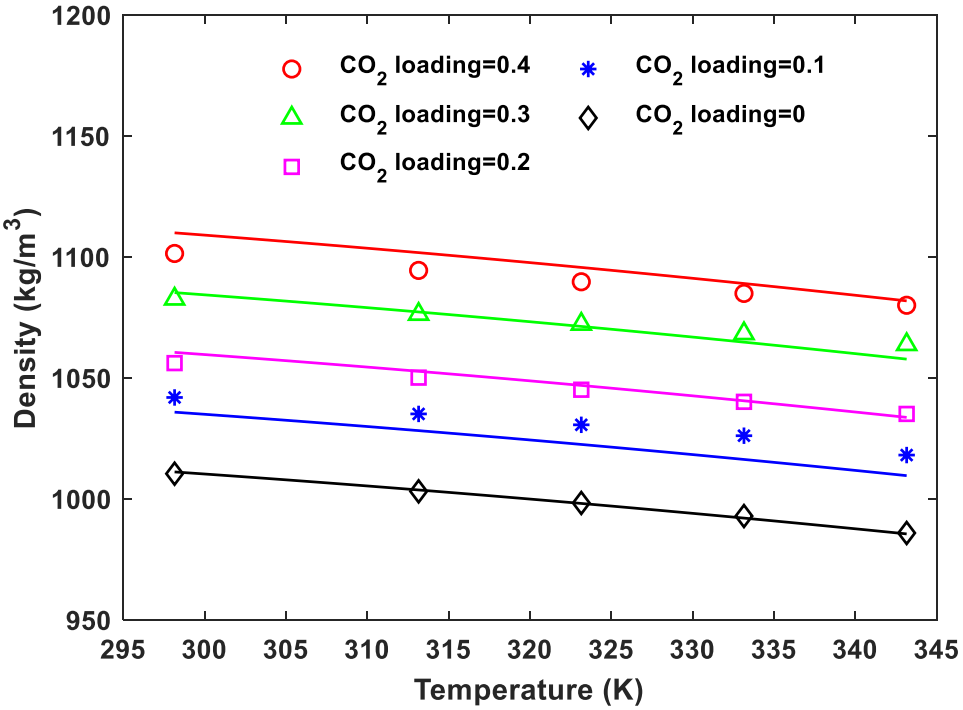

Fig. 7 The effect of CO_2 loading capacity on density of 30 wt% MEA solution. Points: experimental data, Lines: calculated from Eq. (33).

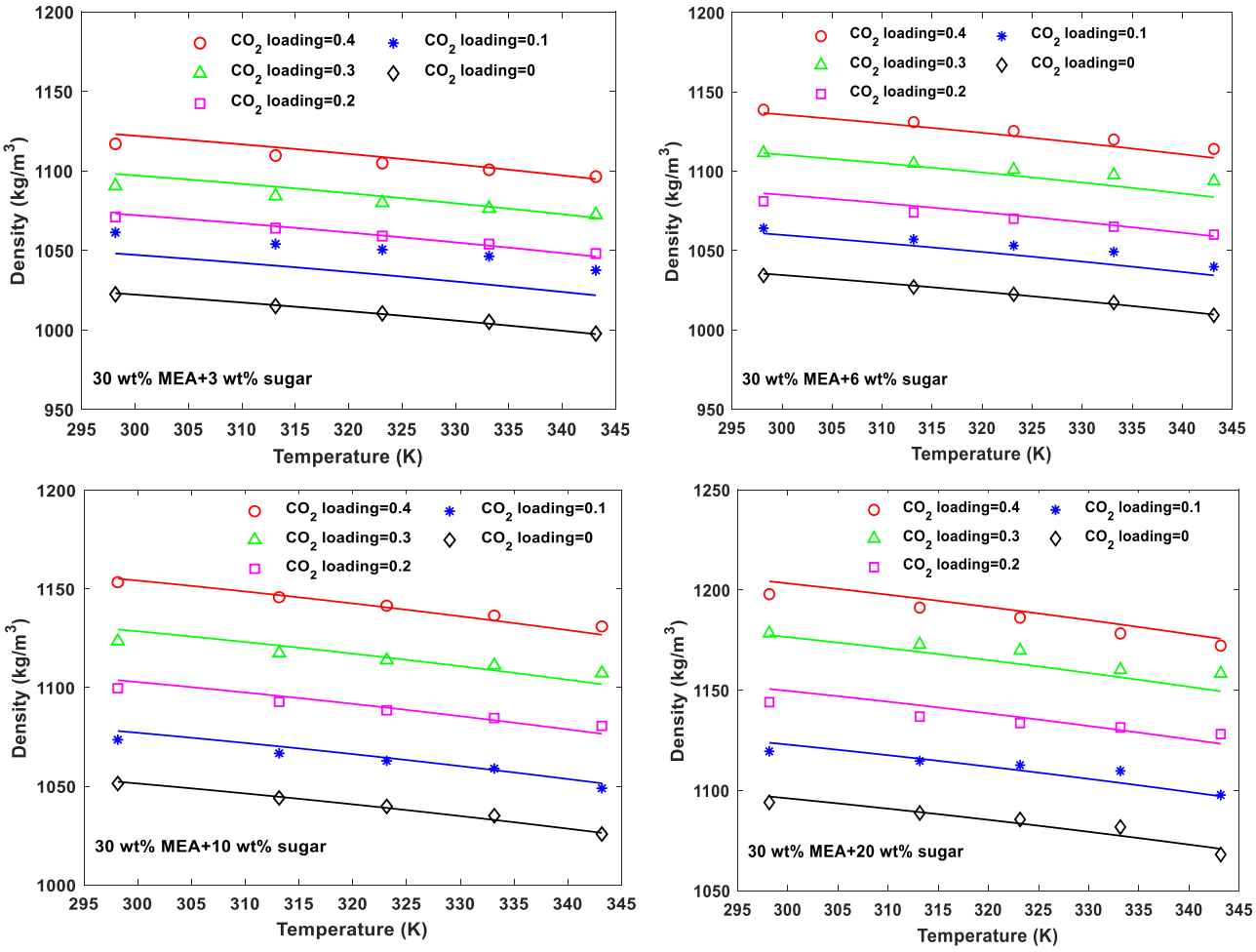

Fig. 8 The effect of CO_2 loading capacity on density of MEA + sugar. Points: experimental data, Lines: calculated from Eq. (33).

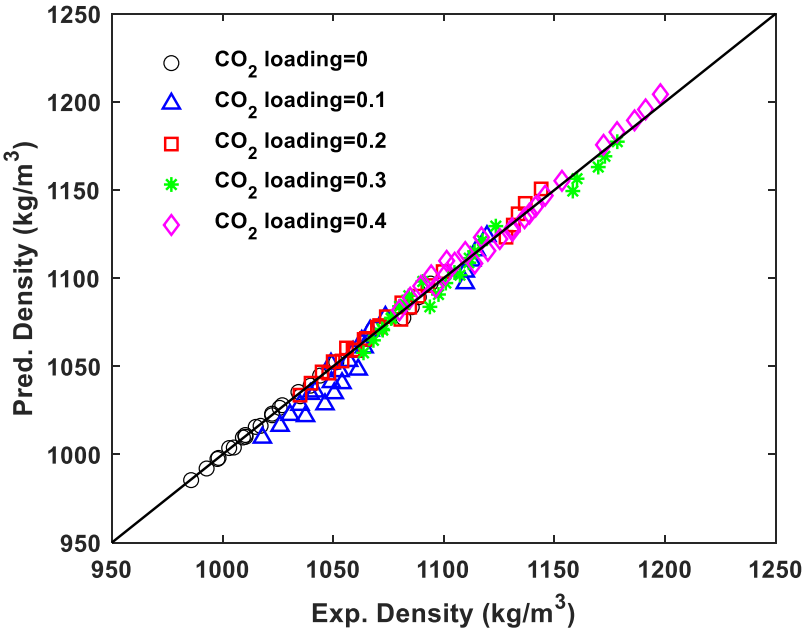

Fig. 9 Parity plot between experimental data and model predicted density of 30 wt% MEA + (0-20) wt% sugar solutions

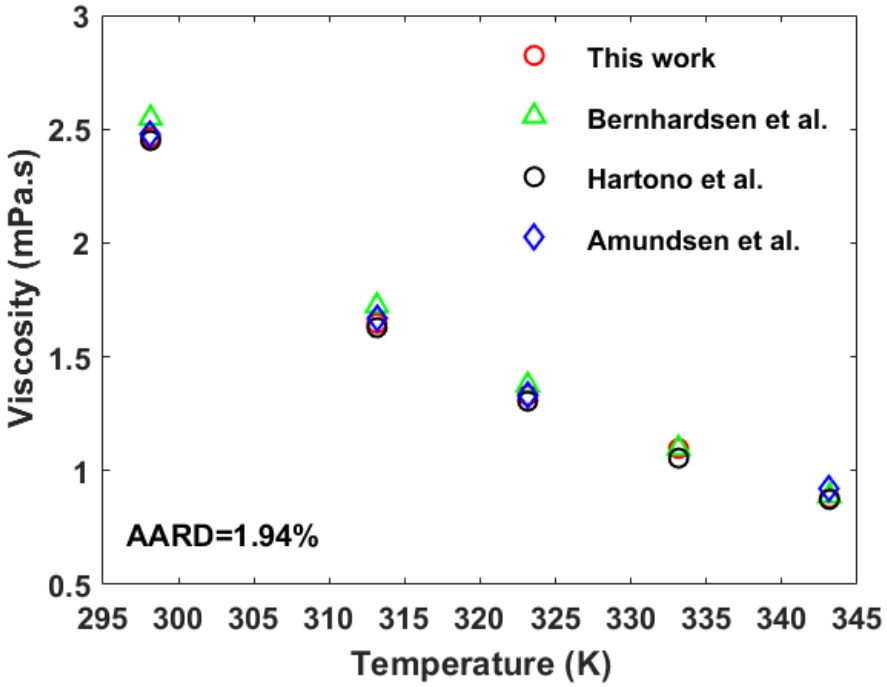

Fig. 10 Viscosity values of 30 wt% MEA measured in this work and reported in the literature

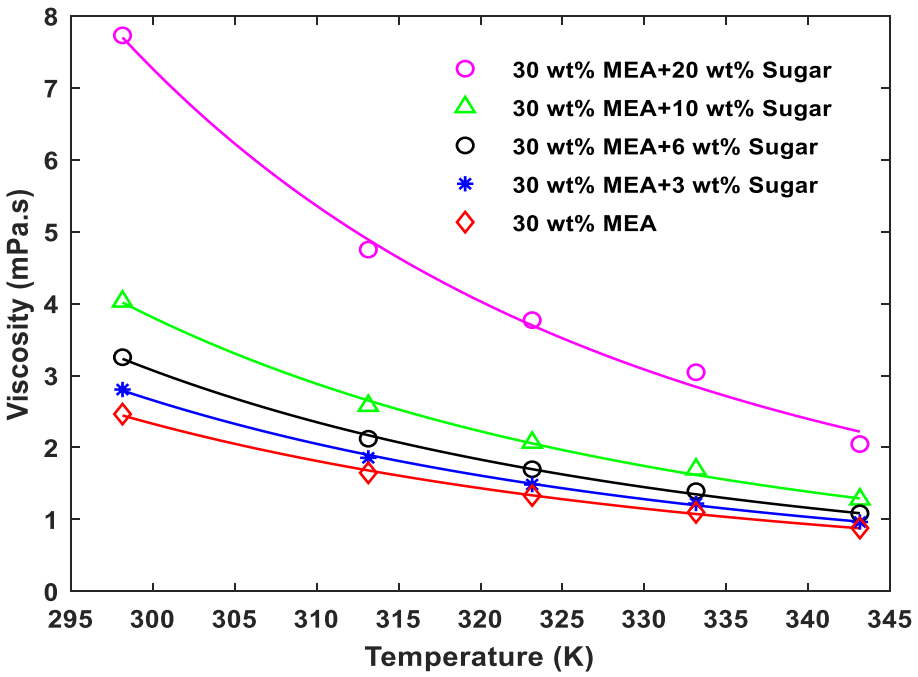

Fig. 11 Viscosity of unloaded MEA and MEA + sugar solutions versus temperature. Points: experimental data, Lines: calculated from Eq. (34).

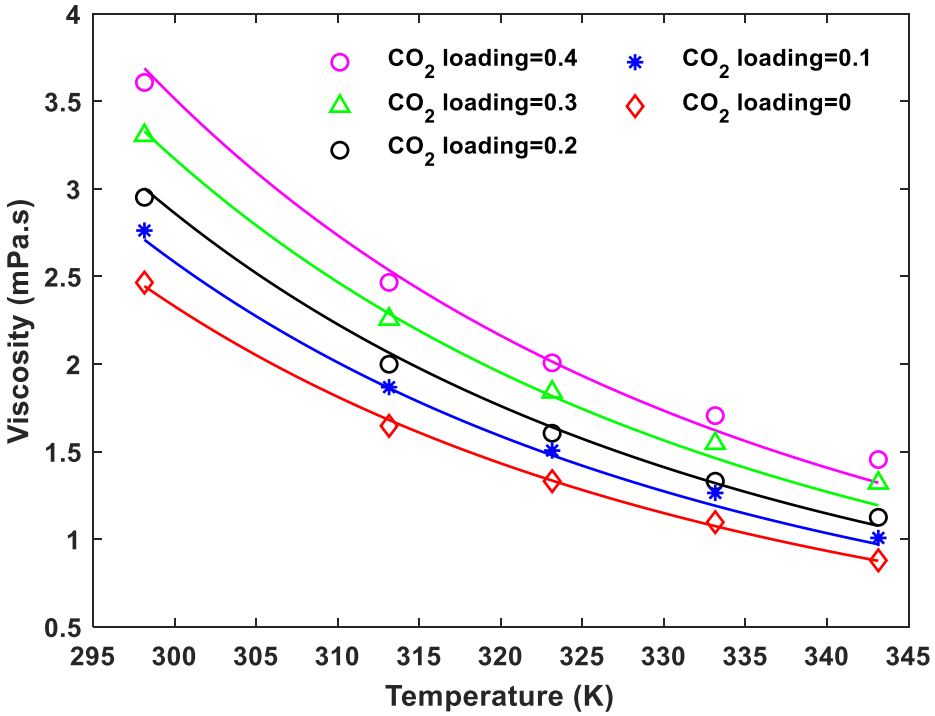

Fig. 12 The effect of CO_2 loading capacity on viscosity of 30 wt% MEA solution. Points: experimental data, Lines: calculated from Eq. (34).

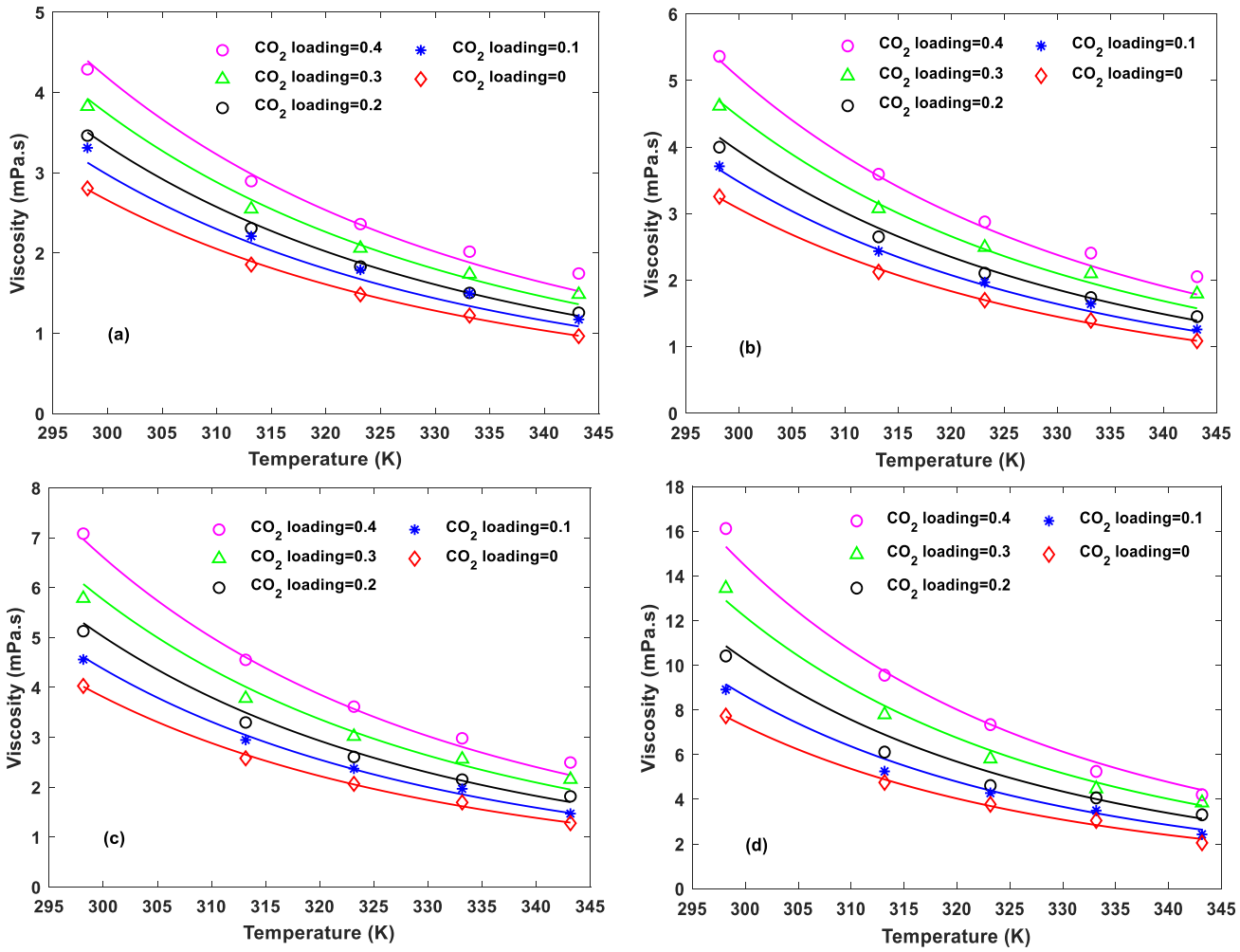

Fig. 13 The effect of CO_2 loading on viscosity of a) 30 wt% MEA + 3 wt% sugar; b) 30 wt% MEA + 6 wt% sugar; c) 30 wt% MEA + 10 wt% sugar; d) 30 wt% MEA + 20 wt% sugar. Points: experimental data, Lines: calculated from Eq. (34).

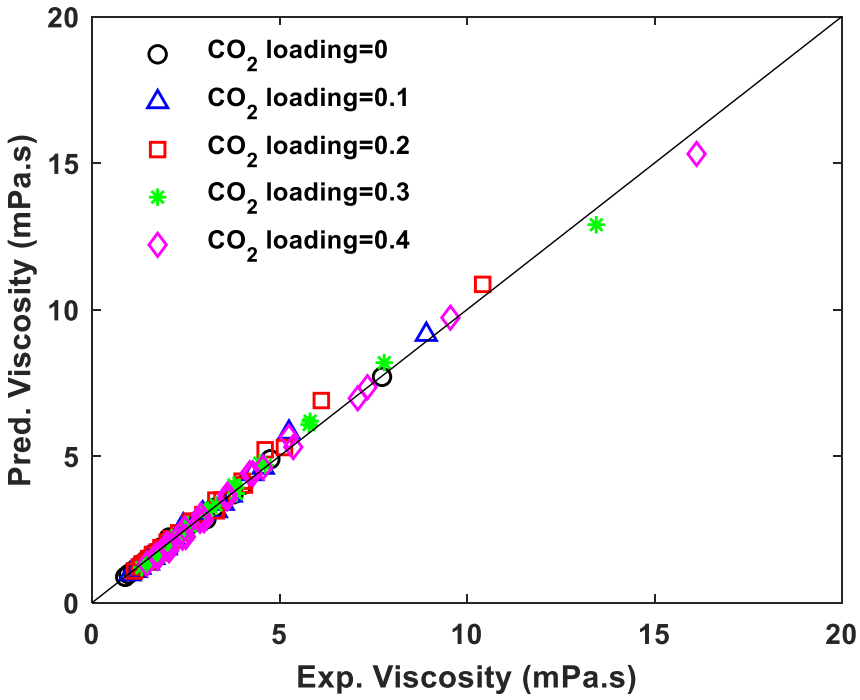

Fig. 14 Parity plot between experimental data and model predicted viscosity of 30 wt% MEA + (0-20) wt% sugar solutions

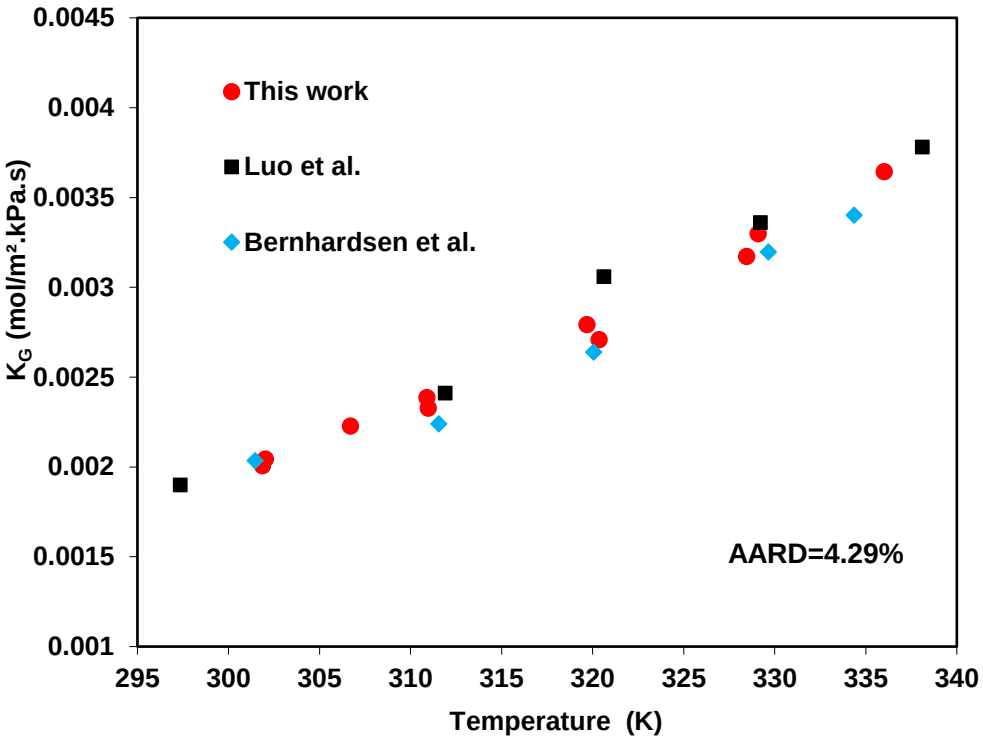

Fig. 15 Comparison of experimental and literature K_G data of 30 wt% unloaded MEA solution.

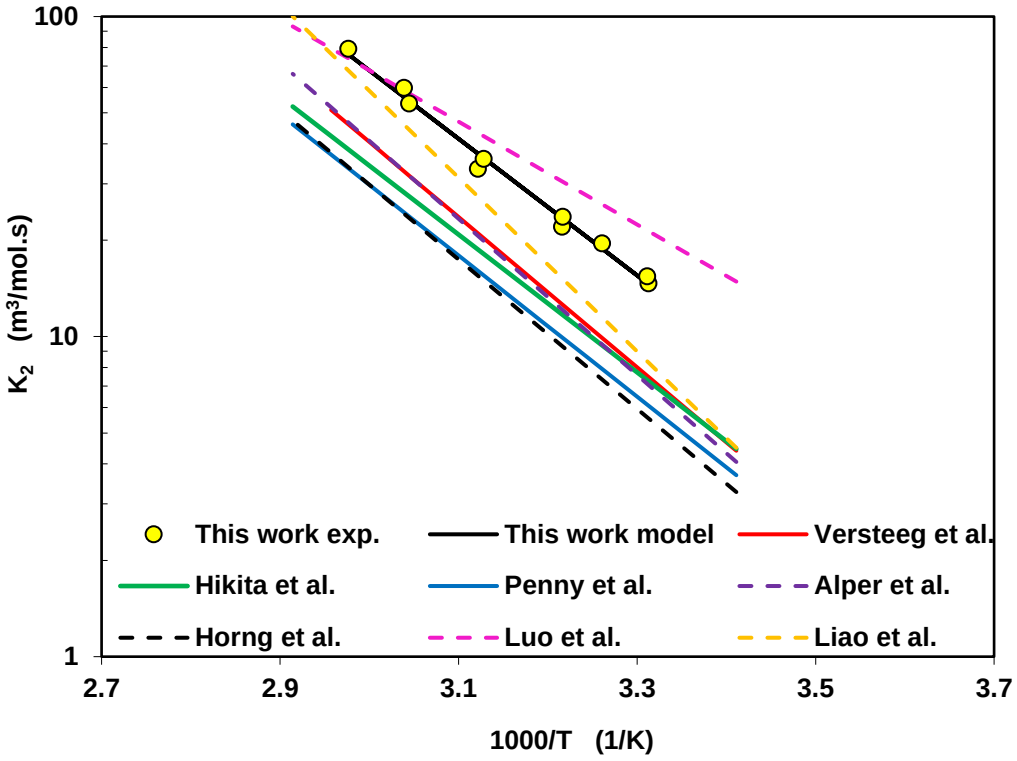

Fig. 16 The second order kinetic rate constant as a function of temperature

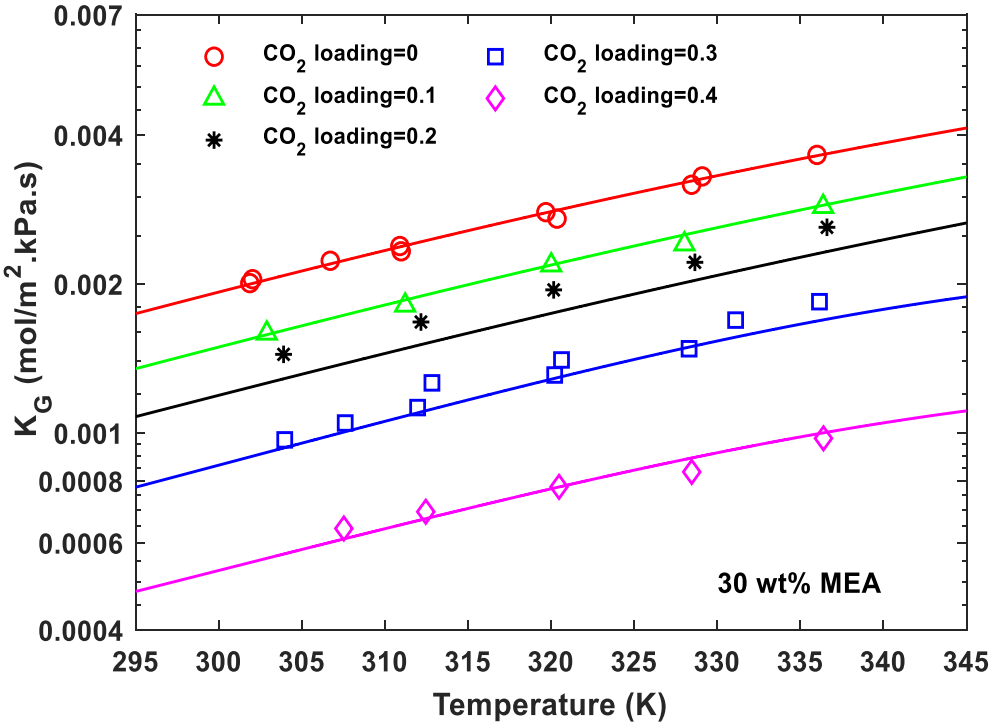

Fig. 17 The effect of CO_2 loading capacity on K_G of MEA solution as a function of temperature.

Points: experimental data, Lines: calculated from model developed in this work.

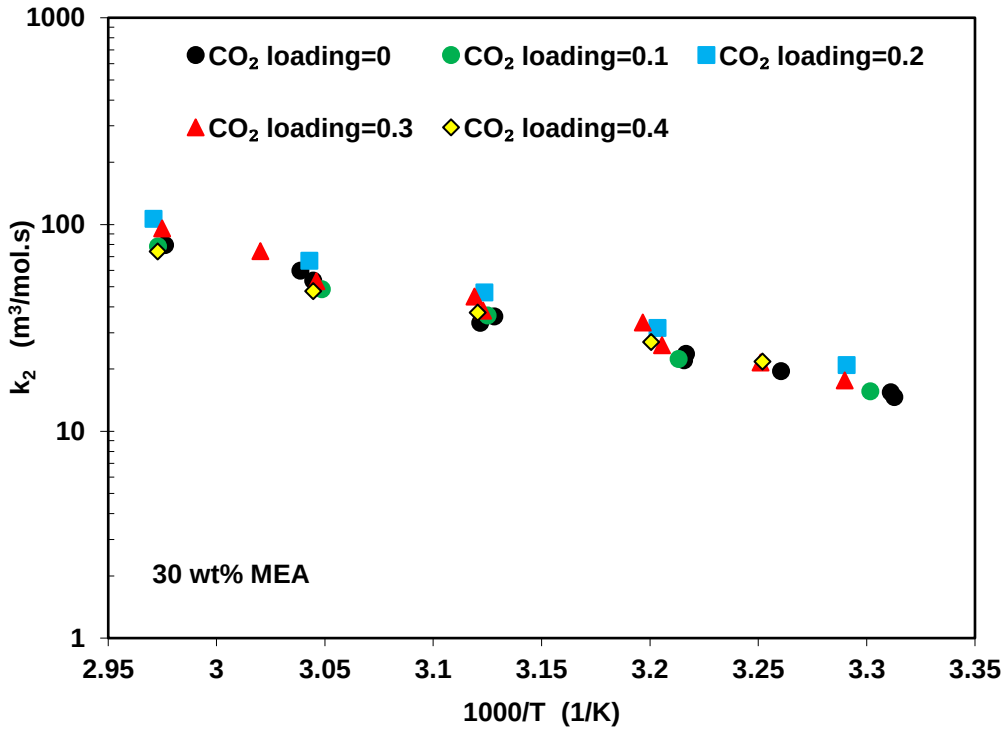

Fig. 18 The effect of CO_2 loading on second order kinetic rate constant in 30 wt% MEA solution

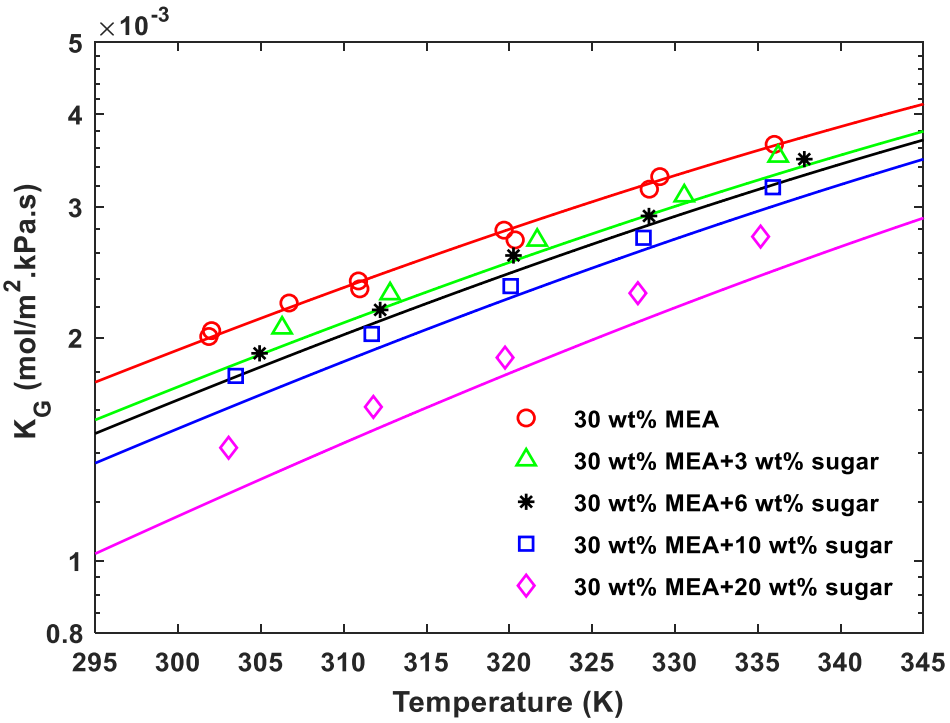

Fig. 19 The effect of viscosity on K_G of unloaded MEA solution as a function of temperature. Points: experimental data, Lines: calculated from model developed in this work.

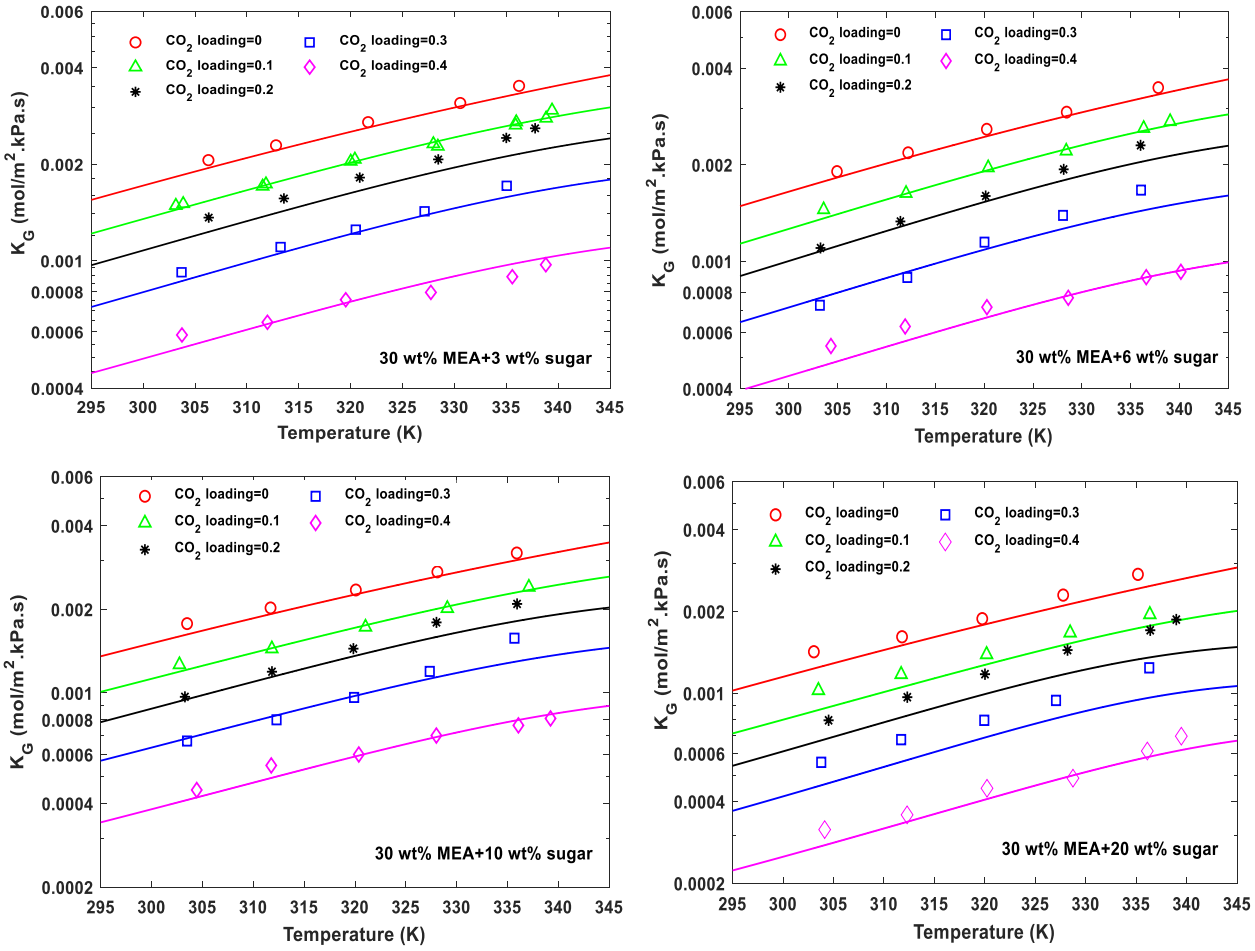

Fig. 20 The effect of CO_2 loading capacity on K_G of viscous MEA solutions. Points: experimental data, Lines: calculated from model developed in this work.

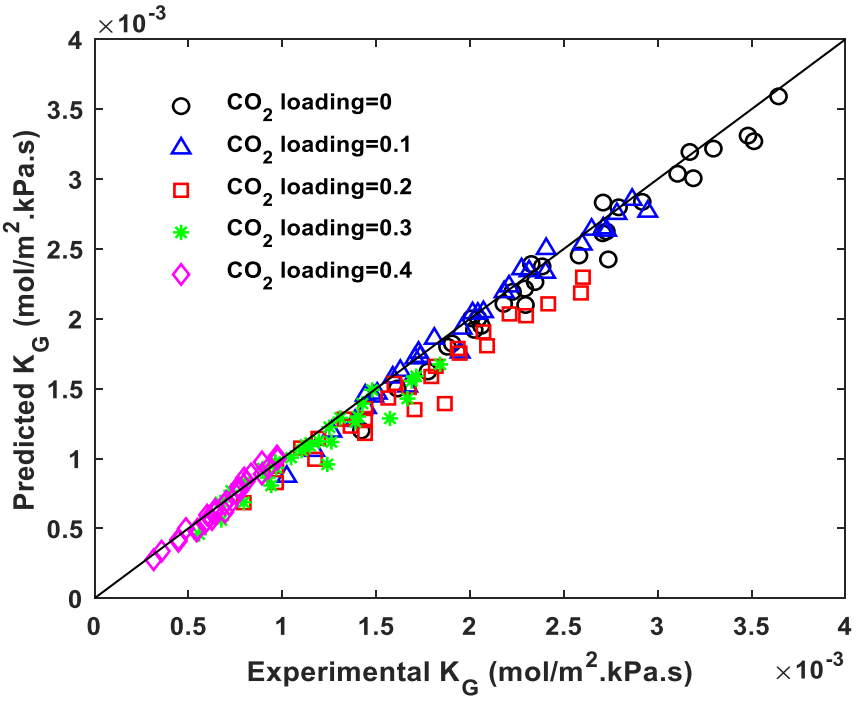

Fig. 21 Parity plot between experimental data and model predicted CO_2 mass transfer for 30 wt% MEA+(0-20) wt% sugar solutions

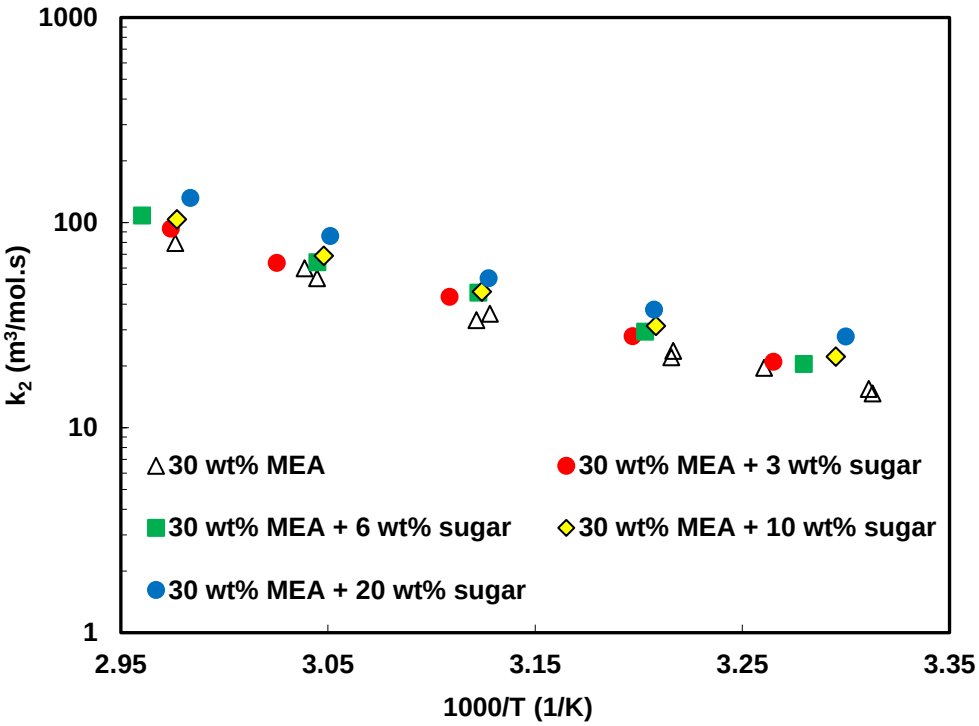

Fig. 22 The second order reaction rate constants in unloaded MEA and viscous MEA solutions

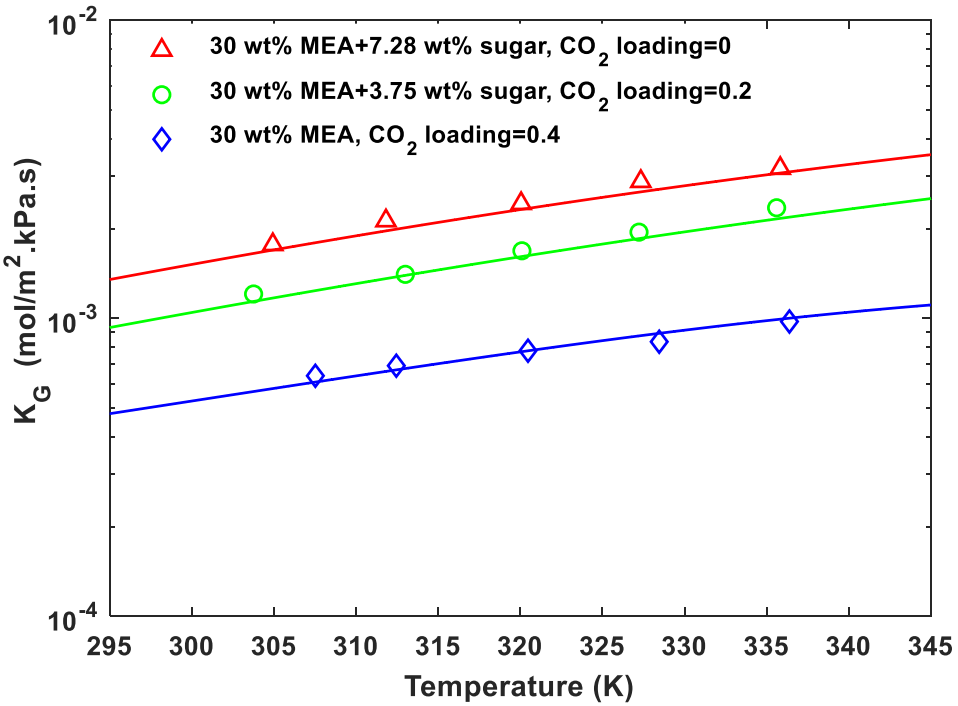

Fig. 23 The effect of CO_2 loading on K_G of MEA solution at constant viscosity. Points: experimental data, Lines: calculated from model developed in this work.

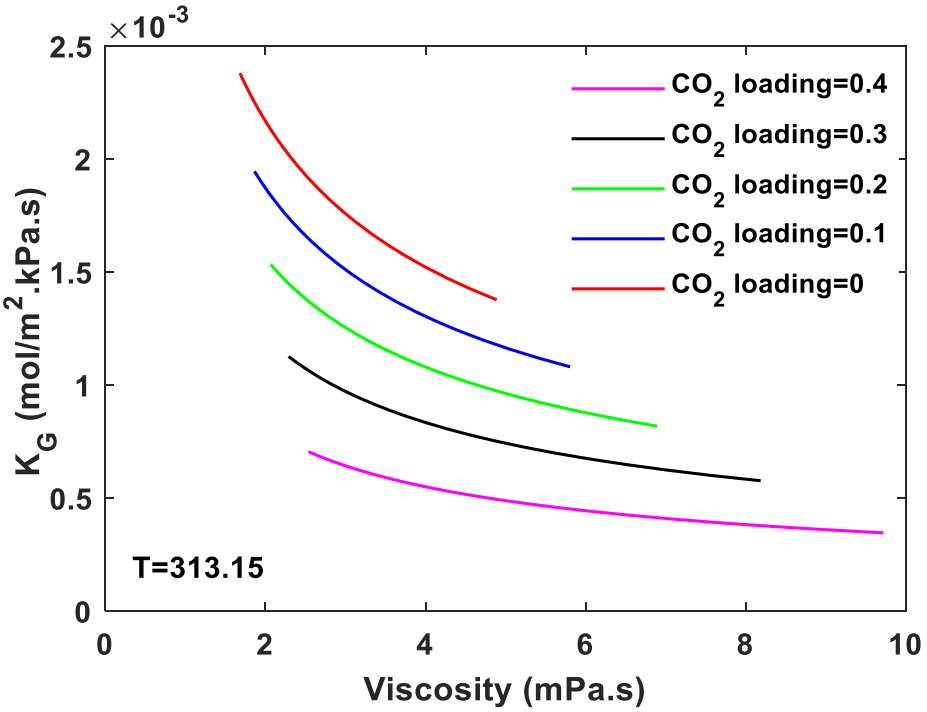

Fig. 24 The overall mass transfer coefficients as a function of viscosity at 313.15 K

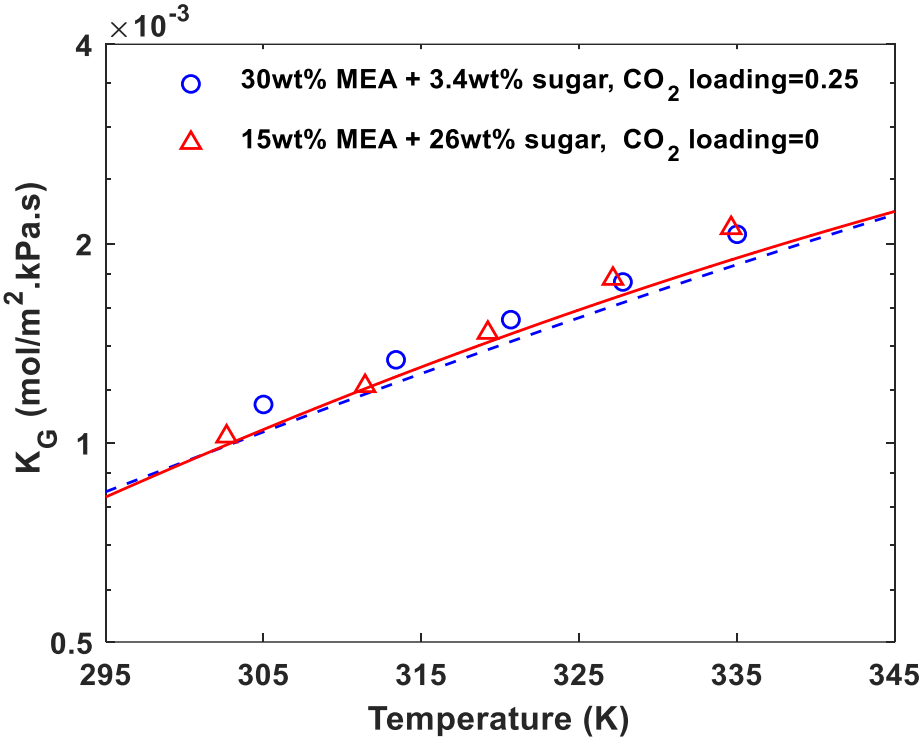

Fig. 25 The overall mass transfer coefficients as a function of temperature. Points: experimental data, Lines: calculated from model developed in this work.

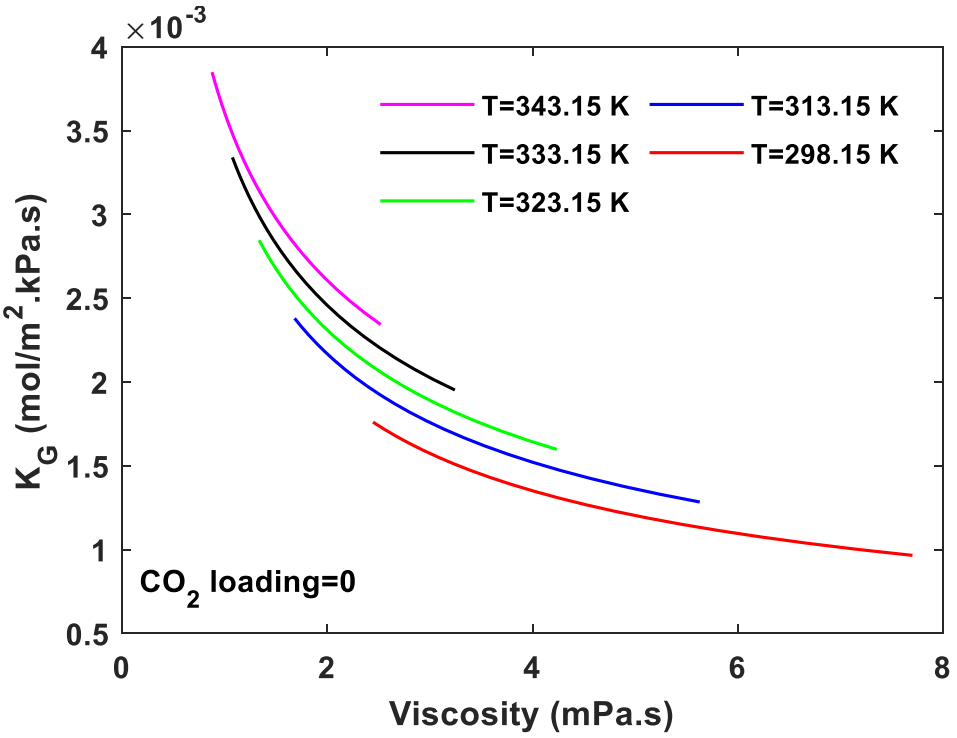

Fig. 26 The overall mass transfer coefficients of unloaded MEA as a function of viscosity